Lawrence Berkeley National Laboratory
Recent Work

Title

REACTIONS OF MODULATED MOLECULAR BEAMS WITH PYROLYTIC GRAPHITE. III HYDROGEN

Permalink

https://escholarship.org/uc/item/6069k9hx

Author

Balooch, M.

Publication Date

1975-08-01

Submitted to Journal of Chemical Physics

LBL-4146
Preprint c.1

REACTIONS OF MODULATED MOLECULAR BEAMS WITH PYROLYTIC GRAPHITE.   III HYDROGEN

M. Balooch and D. R. Olander

August 1975

DISCLAIMER

REACTIONS OF MODULATED MOLECULAR BEAMS WITH PYROLYTIC GRAPHITE. III HYDROGEN
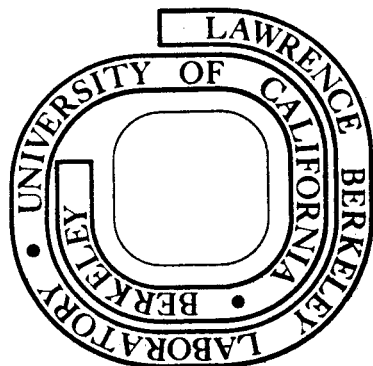
by
M. Balooch and D. R. Olander
Inorganic Materials Research Division of the Lawrence Berkeley
Laboratory and the Department of Nuclear Engineering, University
of California, Berkeley, CA 94720

ABSTRACT

The reaction of hydrogen and pyrolytic graphite was studied by modulated molecular beam-mass spectrometric methods. Because molecular hydrogen does not react with graphite (within the detection limits of the technique), an atomic hydrogen reactant beam was generated by thermal dissociation of H_2 in an effusion oven. At temperatures up to 800°K, methane was the sole product. Acetylene was observed at temperatures above 1000°K. Between 800 and 1000°K, no carbon gasification occured; the surface acted only to recombine H atoms to form H_2. The data were analyzed in terms of a model in which methane is formed by sequential addition of H atoms to CH_n (n = 0,1,2,3) and acetylene is formed by surface combination of two CH groups. The agreement between the model and the molecular beam data is very good. The model also predicts previous high pressure (1 atm H_2) carbon gasification rates determined in conventional kinetic experiments.

I. INTRODUCTION

Over one hundred years have elapsed since Bertholet[1] first investigated the thermodynamics of the carbon-hydrogen system, and four decades have passed since Barrer's classic kinetic study of this system appeared[2,3,4]. The voluminous literature on this subject since these early investigations has been reviewed in a separate document[5]. Recently, the graphite-hydrogen reaction has assumed an important role in several energy production technologies, in particular production of inexpensive heating gas by coal gasification, and graphite corrosion in the high temperature gas cooled reactor and of first wall liners in the controlled thermonuclear reactor.

All previous studies of the carbon-hydrogen reaction have been of the conventional chemical kinetic type. Hydrogen gas at pressures ranging from a few torr to tens of atmospheres is passed over a sample of carbon held at temperatures between 600 and 2600°C. Usually the sole measure of the reaction rate is sample weight loss, although occasionally the quenched gases are analyzed for methane, acetylene and higher hydrocarbons. The specimens are in the form of tubes, bulk shapes, fine filaments, or powders in a packed bed. The types of carbon range from amorphous to graphitic. Even among the graphites, the reaction kinetics are quite sensitive to the purity and degree of crystallinity of the sample. It is not surprising that the apparent reaction rate constant obtained from these data and the equation:

$$\text{rate} = k_{app} p_{H_2} \qquad (1)$$

where p_{H_2} is the hydrogen pressure, differ by as much as five orders of magnitude at the same temperature. There is no established mechanism of the reaction.

In the present investigation, the reaction specimens are high-temperature annealed pyrolytic graphite in either the basal or prism plane orientations. The molecular beam-mass spectrometric technique utilized the graphite oxidation studies described in Parts I and II of the series[6,7] are employed in the hydrogen investigation. Contrary to oxygen, the molecular form of hydrogen is very unreactive towards graphite. The inertness of H_2 is due to the very low probability of dissociative adsorption of the diatomic molecule on graphite surfaces. To render the reaction detectable in the molecular beam system, atomic hydrogen is used as the reactant gas. Thermal dissociation of H_2 prior to striking the graphite target greatly increases the sticking probability but does not influence the course of the subsequent surface reactions which ultimately lead to gaseous hydrocarbon products.

II. EXPERIMENTAL APPARATUS

A. General

The general features of the apparatus (Fig. 1), and of the species detection, signal processing and data analysis methods have been described in detail elsewhere[3]. A mixture of atomic and molecular hydrogen effusing from a hot oven source is chopped by a rotating disk and collimated into a collision-free beam which is ∿3mm diameter as it strikes the graphite target. Reflected H and H_2 and any reaction products emitted from the target

are sampled by another collimator separating the target chamber and the chamber housing the mass spectrometer. The mass spectrometer output signal is fed into a lock-in amplifier where it is combined with a reference signal derived from the chopper motor. Each experimental point consists of the amplitude and phase angle of a selected reaction product and of atomic hydrogen. The ratio of the signal amplitude of the reaction product to that of the reflected hydrogen is denoted as the apparent reaction probability. The phase difference between the reaction product and reflected H atom signals is called the reaction phase lag. These two experimental quantities are corrected for various parasitic effects[8] and the ratio of the ionization cross section of the reaction product to that of atomic hydrogen before comparison with theory. Apparent reaction proabilities and reaction phase lags are measured as functions of the modulation frequency, the target temperature, and the atomic hydrogen beam intensity.

The pyrolytic graphite wafers with prism or basal planes parallel to the reacting surface were obtained from the Union Carbide Company. The specimens had been annealed at 3000°C for several hours (by the manufacturer) to increase the crystallinity and the density (the latter is 99.5% of the theoretical value in our samples). The specimens are thinned to prescribed size (1mm or 25μm thick) and mechanically polished prior to insertion in the vacuum system. The sample is baked at ∿500°K for 1 day and annealed at 1500°K for a few hours before each experiment. All data were collected on a single sample of each crystallographic orientation.

-3-

B.   Atomic Beam Source

The reaction probability of molecular hydrogen with pyrolytic graphite is well below the sensitivity limit of our apparatus (minimum detectable reaction probability $\sim 10^{-5}$). Consequently, we constructed a high-temperature furnace for producing a beam of atomic hydrogen (see Fig. 2). A tungsten tube, closed at one end, was fabricated by chemical vapor deposition. The outer diameter of the tube is 0.37cm, the wall is 0.25mm thick and the length is 7cm. A 1mm diameter orifice is spark-cut into the wall at about the midplane. The open end of the tube is press-fit into a water cooled copper block into which a copper tube for gas supply is brazed. The tube is heated resistively by current passing through six tungsten leads (0.76mm diameter) which are wound around and spring-loaded to the bottom of the tungsten tube. In this way, no significant bending moment is applied to the tungsten tube, which is essentially free-hanging. When heated, the tube expands axially by sliding down through the spiral of tungsten wire leads. The electrical resistance of the tube is higher than that of the leads, so that the maximum temperature occurs near the tube midplane where the orifice is located. The temperature is measured by sighting an optical pyrometer directly into the effusion hole. The temperature is quite uniform along most of the tube length. The maximum usable temperature is $\sim 2500°K$, which is achieved with 150 amps of current and 0.75kW of power. Heat loss is minimized by cylindrical radiation shields around the tungsten tube. To prevent overheating of the chopper motor by the oven assembly, the chopper disk is gold-plated for high reflectivity.

The partial pressure of atomic hydrogen in the oven as a function of total hydrogen pressure (measured in the inlet gas supply) and temperature can easily be calculated if thermodynamic equilibrium is assumed. By measuring total hydrogen pressure in the source and the mass spectrometer signals for reflected H and H_2 (correcting for ionization cross section ratios), the partial pressure of atomic hydrogen in the oven can be determined experimentally. This determination does not require absolute calibration of the mass spectrometer for H or H_2. Comparison of the experimental performance of the oven with equilibrium theory is shown in Fig. 3 for a temperature of 2500°K. The good accord suggests that thermodynamic equilibrium prevails in the oven. Knowing the partial pressures, the fluxes of atomic and molecular hydrogen from the orifice and the beam intensity at the target can be computed from simple kinetic theory.

The strength of the atomic hydrogen beam which can be produced by the oven is limited by the ability of the diffusion pump on the source chamber to handle the gas load. This limit is reached when the feed hydrogen pressure to the source tube is ∼6 torr. At this pressure and 2500°K, the partial pressure of atomic hydrogen is ∼1.5 torr and the intensity of the atomic hydrogen beam striking the target is ∼8.5×10^{16} atoms/cm^2-sec. This flux is equivalent to an isotropic atomic hydrogen gas at a pressure of 5×10^{-4} torr and 2500°K. The molecular hydrogen contaminant in the beam has no effect on the surface reactions; it simply scatters from the surface as would a rare gas.

III. RESULTS

A. Surface Morphology

Figure 4 shows scanning electron micrographs of basal and prism plane specimens used in this investigation. The two top micrographs show the surface structures after polishing. The bottom photographs show the condition of the targets after the experiments. Contrary to the case of oxygen attack[6], the basal plane surface (Fig. 4c) is little affected by reaction with atomic hydrogen, which produces a uniform recession. The structure of the retired prism plane (Fig. 4d) is characterized by extensive ridging parallel to the basal planes. A similar type of structure was observed on samples which had been reacted with oxygen[7]. However, we have ascertained that the ridges are not caused by reaction of hydrogen. Similar morphology is found on regions of the surface which had been heated but which were not illuminated by the primary hydrogen beam. It appears that heat treatment, not chemical reaction, is responsible for the ridged structure.

B. Nature and Temperature Depenedence of the Reaction Products

Only two reaction products, both stable hydrocarbons, were observed over a temperature range from 400 to 2200°K. The apparent reaction probabilities for methane (ϵ_{CH_4}) and acetylene ($\epsilon_{C_2H_2}$) are shown in Fig. 5 as functions of graphite temperature (T_s). In this series of experiments, the beam intensity was 8×10^{16} H atoms/cm^2-sec and the modulation frequency was 20Hz. The temperature of the H atom beam in all experiments reported in this paper was 2500°K.

In detecting methane, the ions CH_4^+, CH_3^+, CH_2^+, and CH^+ were observed. However, all of these ion signals exhibited the same temperature dependence and phase lag, and it was concluded that all arose from CH_4, the last three being fragments from dissociative ionization in the mass spectrometer. For convenience, the methane data were actually determined by measurement of the CH_3^+ signal, which was found to be freer of noise than the CH_4^+ peak. All methane reaction probabilities reported here were corrected for the observed cracking pattern.

The most striking features of the data shown in Fig. 5 are the small number of products and the clean separation of methane and acetylene with temperature. Below 800°K, methane is the only detectable reaction product. The methane signals increased with decreasing temperature and appeared to be approaching a plateau at low temperatures. Methane was observed as a bona fide reaction product at the lowest temperature attainable in this apparatus, which is somewhat greater than 400°K (even with the target heater off, the sample was heated by the hydrogen oven in the source chamber). This "room temperature" reaction was observed in the oxygen-graphite reaction[7]. The methane data in Fig. 5 are in very good agreement, both in magnitude and in temperature depen- dence, with the data obtained by Rosner and Allendorf[9] in their study of the kinetics of discharge-produced atomic hydrogen with isotropic graphite.

Above 1000°K, only acetylene was observed and its production rate increased rapidly with temperature up to the maximum attainable (2200°K). Between 800°K and 1000°K, no gasified carbon products were detected. In this region, the graphite surface simply acts

as a catalyst to recombine adsorbed H atoms to form H_2. We could not detect this product above the strong signal due to undissociated H_2 reflected from the primary beam.

The results shown in Fig. 5 indicate that, as expected, the prism plane of graphite is more reactive than the basal plane.

At the same time that the reaction probability measurements shown in Fig. 5 were obtained, the reaction product phase lags for methane and acetylene (ϕ_{CH_4} and $\phi_{C_2H_2}$) were also recorded. These data are shown in Fig. 6. The most interesting feature of these results is the difference in the variation of ϕ_{CH_4} with temperature for the different surface orientations. The ability to predict this fine structure is a good test of any surface mechanism applied to this system.

C.   Frequency Dependence

Figures 7 and 8 show the variation of the phase lag and apparent reaction probability for methane with frequency at a fixed beam intensity and surface temperatures in the neighborhood of 500°K. Note the inversion of the magnitudes of ϕ_{CH_4} and ε_{CH_4} with respect to surface orientation; the prism plane exhibits larger reaction probabilities than the basal plane but the phase lag is larger for methane produced from the basal plane than from the prism plane. Similar frequency data for acetylene reaction product are shown in Figs. 9 and 10. The phase-frequency data in Figs. 7 and 9 suggest that processes other than purely surface

reactions are involved in the mechanism. In particular, the very slow change in phase lag with frequency and the inability to attain close to zero phase lag at high temperature and low modulation frequency suggest that bulk solution-diffusion is important in the graphite-hydrogen reaction.

D.   The Effect of Beam Intensity

The variations of ε and ϕ with beam intensity were determined for the methane product at low temperature (Figs. 11 and 12) and for acetylene at high temperature (Figs. 13 and 14). Since for a linear reaction mechanism, phase lag and reaction probability are independent of beam intensity, it is clear that the surface mechanism responsible for the production of both products is nonlinear. Figures 12 and 14 indicate that the reaction order is greater than unity for both reaction products.

E.   Effect of Target Thickness

Up until this point, the results have been reported for targets 1mm thick. To ascertain the effect (if any) of target thickness, which might affect bulk diffusional component of the reaction mechanism, we polished one of the basal plane specimens to a thickness of 25μm. Figures 15 and 16 compare the reaction probabilities and phase lags on the thick and thin targets. For the two targets studied there is no discernible effect of target thickness on the reaction product characteristics.

F.   Hysteresis

The hysteresis effect observed in the earlier oxygen-graphite study[6] was also found in the present reaction. The methane reaction probability follows the upper curve in Fig. 17 as the temperature is increased from 400°K to the temperature at which the signal is indistinguishable from the noise (800°K). If the target temperature is decreased from this point, the reaction probability retraces the upper curves. However, if the target temperature is raised to ∿2000°K instead of stopping at 800°K, the lower curve in Fig. 17 (open circles) is followed. The hysteresis loop is more easily closed at its high temperature end in the case of hydrogen attack than for oxidation[6]. Throughout the present study, we tried to avoid the hysteresis effect by high temperature annealing before each experiment, which should place the data consistently on the lower curve of Fig. 17 (or its analog for other types of experiments).

IV.   SURFACE REACTION MODEL

A.   General Features

As indicated in ref. (8), the method of deducing a mechanism to explain the observed variation of ϵ and ϕ for each reaction product with target temperature (T_s), beam intensity (I_0) and modulation frequency (ω) involves assuming a model, analyzing the model for the predicted ϵ and ϕ and comparing the predictions with the data. The best model is the one which fits all of the data with equal accuracy. To reduce the number of iterations of this process, the following qualitative features of the data

suggest important ingredients of the mechanism:

1.   The clear separation in temperature between regimes of methane production, recombination, and acetylene production (Fig. 5) implies that the activation energies for the elementary steps involved must be smallest for methane production, intermediate for recombination, and largest for acetylene production.

2.   The fact that the beam intensity affects ϵ and ϕ (Figs. 11-14) immediately requires a nonlinear mechanism for both hydrocarbon products. Moreover, the elementary steps for both products must be combined in a way which produces an overall reaction order greater than unity.

3.   The sluggish response of the phase lag as the modulation frequency is changed (Figs. 7 and 9) suggest that bulk diffusion (probably of hydrogen, which is common to both CH_4 and C_2H_4 production) is an important step in the reaction model at all temperatures. In addition, the fact that target thickness does not influence the acetylene results (Figs. 15 and 16) indicates that the target may be modeled as a semi-infinite medium in the diffusional part of the theory.

The following mechanism reflects the general features of the data described above. The H_2 component of the primary reactant beam is totally reflected from the surface. Some of the hydrogen atoms in the beam adsorb with a sticking probability η. The adsorbed H can dissolve and diffuse into and out of the bulk solid. There are three routes by which adsorbed H atoms are

-11-

returned to the vacuum:

(a)   By a series of elementary steps culminating in CH_4 production. These steps are postulated to consist of sequential additions of adsorbed H atoms to CH_n (n=0,1,2,3) surface species. This branch is active at low temperatures.

(b)   By direct recombination of adsorbed H atoms to form H_2 which immediately leaves the surface.

(c)   By reaction between two CH radicals on the surface to form acetylene. This branch becomes important only at temperatures above 1000°K.

The mechanism is shown in detail in Fig. 1. Some characteristics of its elementary steps are described below:

Sticking of atomic hydrogen: The sticking probability is assumed to be temperature independent. Because the methane branch removes adsorbed hydrogen from the surface even at low temperatures, the concentration of adsorbed hydrogen is presumed to remain low enough so that coverage dependence of the sticking process is negligible. This assumption can be verified after the parameters of the model have been fitted to the data and absolute magnitudes of the concentration of adsorbed hydrogen are calculated from the model.

Bulk solution and diffusion: The most likely species to dissolve and diffuse in bulk graphite is atomic hydrogen. Because of the small size of this species, diffusion is assumed to occur in the graphite lattice. The assistance of grain boundary diffusion (as was found to be necessary in the oxygen-graphite reaction[7]) need

-12-

not be invoked to explain the hydrogen-graphite reaction. Simple lattice diffusion of H in graphite with a diffusion coefficient denoted by D is sufficient for the present analysis. Equilibrium between the adsorbed hydrogen and the hydrogen dissolved in the solid just beneath the surface is also assumed. There is no way of verifying this last assumption, but if it were not made, many more kinetic constants would appear in the analysis and require fitting to the data.

Surface recombination: The H atoms on the surface are assumed to be mobile at all surface temperatures, and collisions between them can lead to formation and escape of H_2.

Surface equilibria: The reaction of adsorbed hydrogen with a surface carbon atom to form CH is assumed to be in equilibrium (equilibrium constant K_1) as is the next H atom addition step to form CH_2 (equilibrium constant K_2). Allowing partial reversibility of these two steps would introduce more kinetic constants into the analysis than can be accurately determined from the data.

Methane production: The slow step in the methane branch is assumed to be the addition of an adsorbed H atom to CH_2 on the surface. Assignment of this slow step is necessary to properly match the reaction order data. The final addition of an H atom to the surface methyl radical to form methane is assumed to be fast.

Acetylene production: At high temperatures, the surface CH species is assumed to become sufficiently mobile to permit collisions between migrating CH species to occur and produce acetylene.

B.   Analysis of the Reaction Model

The surface concentration of adsorbed hydrogen atoms is denoted by $n(t)$ and the concentration of this species in the bulk solid by $C(x,t)$, where x is the distance in the penetration depth normal to the surface and t is the time. The bulk concentration of hydrogen just beneath the surface is assumed to be related to the concentration of adsorbed hydrogen by the solubility coefficient H:

$$C(0,t) = Hn(t) \tag{2}$$

The diffusion equation for hydrogen in the bulk is:

$$\frac{\partial C}{\partial t} = D \frac{\partial^2 C}{\partial x^2} \tag{3}$$

Of the two boundary conditions needed to solve Eq. (3), one is obtained from the assumption of a semi-infinite medium:

$$C(\infty, t) = \text{finite} \tag{4}$$

The second boundary condition is obtained from a mass balance on surface hydrogen. Using Eq.(2) to eliminate $n(t)$ from this balance yields:

$$\frac{1}{H} \frac{dC(0,t)}{dt} = nI_o g(t) - 2(k_2^e + K_1^2 k_2)\frac{[C(0,t)]^2}{H^2} - 4K_1 K_2 k_3 \frac{[C(0,t)]^3}{H^3}$$

$$+ D\left(\frac{\partial C}{\partial x}\right)_{x=0} \tag{5}$$

Here I_o is the beam intensity (dc) and $g(t)$ is the gating function of the beam chopper, which is the fraction of the maximum (dc) beam flux passed by the chopper at time t. The first term on the right hand side of Eq. (5) represents the rate of adsorption of H atoms per unit surface area from the primary beam. The second term is

due to the loss of hydrogen by the combined effects of recombination and acetylene formation. The third term represents methane production. In forming the hydrocarbon production terms in the mass balance, the concentration of surface CH is equal to $K_1 n$ and that of CH_2 is given by $K_1 K_2 n^2$. The last term on the right hand side of Eq. (5) represents diffusion into and out of the bulk solid. In deriving Eq. (5), we have made the assumption that the surface concentration of H is much greater than that of CH or CH_2.

Equation (5) clearly displays the nonlinearity of the proposed mechanism. The conventional way to treat nonlinear problems of this sort is first to solve the equations in the time domain (which usually requires numerical solution except in a few simple cases, of which the present mechanism is not one) and then to Fourier analyze the product flux waveform for the phase and amplitude of the fundamental mode[10,11]. To avoid this laborious procedure, we use the approximate treatment of nonlinear problems outlined in ref. (12). In this work, it was determined that application of the approximate method to the pure third order desorption problem (i.e., Eq. (5) with the second order and diffusion terms omitted) produces amplitudes which are within 6 % of those computed from the exact solution and phase lags which are accurate to within 4°. Because the present problem includes first and second order processes in addition to the third order step, the accuracy of the predicted phase lags and reaction probabilities from the approximate method will be higher than in the case of pure third order reaction. The accuracy is certainly within the precision of the data, so that we have no reservations

about exploiting the simpler approximate method. Following to
the procedure described in ref. (12), the beam gating function
is written as:

$$g(t) = \frac{1}{2}[1 + g_1 e^{i\omega t}] \tag{6}$$

where ω is the modulation frequency in radians/sec, and the
concentration $C(x,t)$ is expanded in the abbreviated Fourier
series:

$$C(x,t) = C_o + C_1(x) e^{i\omega t} \tag{7}$$

Substituting Eq. (7) into Eq. (3) and solving the resulting
ordinary differential equation for $C_1(x)$ yields:

$$\overline{C}_1(x) = \overline{C}_1(0) \exp\left[-\left(\frac{i\omega}{D}\right)^{1/2} x\right] \tag{8}$$

where Eq.(4) has been used to eliminate the exponential solution
with the positive argument. The unknown quantity $\overline{C}_1(0)$ is
determined by substituting Eqs. (6)-(8) into Eq. (5). The
coefficients of the zeroth and first powers of $\exp(i\omega t)$ in the
resulting algebraic equation are collected and equated independ-
ently to zero. This procedure determines C_o and $\overline{C}_1(0)$ by the
equations:

$$4K_1 K_2 k_3 \left(\frac{C_o}{H}\right)^3 + 2(k_2^e + K_1 k_2) \left(\frac{C_o}{H}\right)^2 = \eta I_o / 2 \tag{9}$$

$$\overline{C}_1(0) = \frac{\eta I_o g_1 H/2}{i\omega + 12K_1 K_2 k_3 (C_o/H)^2 + 4(k_2^e + K_1^2 k_2)(C_o/H) + (i\omega H^2 D)^{1/2}} \tag{10}$$

The rate per unit area of product emission is $K_1 K_2 k_2 n^3$ for
methane and $K_1^2 k_2 n^2$ for acetylene. These product desorption rates
are referenced to the flux of hydrogen atoms impinging on the

target, which is $I_0 g(t)$. Expressing n in terms of $C(0,t)$ by Eq. (2) and using Eqs. (6) and (7) for $g(t)$ and $C(0,t)$, respectively, the reaction product vectors are:

$$\epsilon_{CH_4} \exp(-i\phi_{CH_4}) = \frac{6K_1 K_2 k_3 C_0^2 \bar{C}_1(0)}{I_0 g_1 H^3} \tag{11}$$

for methane, and:

$$\epsilon_{C_2H_2} \exp(-i\phi_{C_2H_2}) = \frac{4K_1^2 k_2 C_0 \bar{C}_1(0)}{I_0 g_1 H^2} \tag{12}$$

for acetylene.

The complete solution to the problem may be obtained by substituting Eq.(10) into Eqs. (11) and (12), converting the complex number in the denominator of Eq. (10) to polar form and identifying the phase lag ϕ and apparent reaction probability ϵ for each product. However, because of the widely separated temperature regions in which the two products are found, the solution for methane may be obtained by neglecting $K_1^2 k_2$ compared to k_2^e in Eq. (10). ϕ_{CH_4} and ϵ_{CH_4} are then found to be:

$$\tan\phi_{CH_4} = \frac{\omega + (H^2 D/2)^{1/2} \omega^{1/2}}{(H^2 D/2)^{1/2} \omega^{1/2} + 4k_2^e(C_0/H) + 12K_1 K_2 k_3 (C_0/H)^2} \tag{13}$$

$$\epsilon_{CH_4} = \frac{3K_1 K_2 k_3 \, n(C_0/H)^2 \sin\phi_{CH_4}}{\omega + (H^2 D/2)^{1/2} \omega^{1/2}} \tag{14}$$

where (C_0/H) is given by solution of Eq. (9) with $K_1^2 k_2$ neglected.

Similarly, in the high temperature region where aceytlene dominates and methane is negligible, $K_1 K_2 k_3$ is set equal to zero in Eqs. (9) and (10) and Eq. (12) yields:

$$\tan\phi_{C_2H_2} = \frac{\omega + (H^2D/2)^{1/2}\,\omega^{1/2}}{(H^2D/2)^{1/2}\,\omega^{1/2} + [4(k_2^e + K_1^2 k_2)I_0\eta]^{1/2}} \qquad (15)$$

$$\varepsilon_{C_2H_2} = \frac{K_1^2 k_2 \eta^{3/2}\, I_0^{1/2}\, \sin\phi_{C_2H_2}}{(K_1^2 k_2 + k_2^e)^{1/2}\,[(H^2D/2)^{1/2}\,\omega^{1/2} + \omega]} \qquad (16)$$

C. Determination of the Constants in the Kinetic Model

The analysis presented in the preceding section results
in predicted values of ϕ and ε as functions of the experimental
variables T_s, I_0 and ω. The model contains 5 explicit parameters,
η, $HD^{1/2}$, $K_1 K_2 k_3$, $K_1^2 k_2$ and k_2^e. The last four of these are
temperature dependent, and if Arrhenius behavior is assumed, each
is characterized by a pre-exponential factor and an activation
energy. Thus, 9 constants for each graphite surface orientation
must be extracted from the data in Figs. 5-13. Note that there
is no way in which the individual thermodynamic parameters (H, K_1,
and K_2) or kinetic parameters (D, k_2 and k_3) can be determined.

Fortunately, the fitting process may be approached piecemeal
so that only a few constants need be considered at one time. The
procedure is as follows:

1)   At the lowest temperature ($T_s \approx 500°K$), where the apparent
reaction probabilities level off (Fig. 5), recombination is
negligible compared to methane production. Here, the methane
data can be analyzed by use of Eqs. (13) and (14) with k_2^e set equal
to zero in conjunction with Eq. (9) in which both k_2^e and $K_1^2 k_2$ are
neglected. $HD^{1/2}$ and $K_1 K_2 k_3$ at $500°K$ are determined by fitting

the ϕ_{CH_4} data in Fig. 7 to Eq. (13). Along with this process, the ε_{CH_4} data in Fig. 8 are utilized to determine the sticking probability. As a result of this procedure, we find the H atom sticking probability on graphite to be 0.02 and 0.006 for the prism and basal plane orientations, respectively. These numbers agree very favorably with the results of Beitel[13]. The lines marked "theory" in Figs. 7 and 8 represent application of Eqs.(13) and (14) with the parameters determined in the manner just described.

2)   An independent check on the model and the parameters determined in step 1 is afforded by the beam intensity effect on the methane data. The lines marked "theory" in Figs. 11 and 12 are plots of Eqs. (13) and (14). No adjustable parameters are available in this comparison. The good agreement shown on the graphs indicates that the modeling process is satisfactory up to this stage.

3)   The Arrhenius parameters of $K_1 K_2 k_3$ and k_2^e are obtained by fitting Eqs. (13) and (14) (with k_2^e retained therein) to the data in Figs. 5 and 6. In this fitting process, the temperature variation of $HD^{1/2}$ over the range $400 < T_s < 800°K$ is neglected. The resulting data-fitting curves are marked "theory" in the methane regions of Figs. 5 and 6. At this point, 5 of the 9 constants have been determined and the value of $HD^{1/2}$ at 500°K is known.

4)   Eq.(15) is fitted to the acetylene frequency scan data in Fig. 9 in order to determine $HD^{1/2}$ and $K_1^2 k_2$ at the single temperature for which these data were obtained (about 2000°K,

-19-

depending on the crystal orientation). The constants avilable
up to here are sufficient to predict the results of the
experiments reported in Figs. 10, 13 and 14. Absolute agreement
of the theory lines with the measurement is excellent (again, no
adjustable parameters are available) so we continue to the final
step.

5) The Arrhenius parameters which determine the temperature
dependence of $K_1^2 k_2$ are obtained by fitting Eqs. (15) and (16) to
the acetylene data in Figs. 5 and 6.

The kinetic parameters of the proposed mechanism are
summarized in Table 2 and presented graphically in Fig. 18. The
agreement between the proposed model (and the measured values
of the constants of its elementary steps) and the data obtained
by the modulated molecular beam technique is very good.

Using these rate constants, Eq. (9) may be utilized to
calculate the average (dc) concentration of adsorbed hydrogen
on the surface (i.e., C_o/H) as a function of temperature. At
the highest beam intensity used in the experiments, the average
surface concentration is less than 3×10^{11} atoms/H cm^2. Since
the density of surface carbon atoms is $\sim 10^{15}$ cm^{-2}, the coverage
is less than $\sim 0.1\%$, which justifies a postiori the neglect of
coverage dependence of the sticking probability. The values of
η given in Table 2 therefore refer to the bare graphite surfaces.

V. DISCUSSION

A. The Reaction Mechanism

The reaction model shown in Table 1 requires substantial mobility of hydrogen atoms on the graphite surface at all temperatures. In addition, the acetylene formation reaction implies surface mobility of the CH species at temperatures above 1000°K.

The hydrogen atom sticking probability is ∿3 times larger on the prism plane than on the basal plane, which is in accord with the commonly observed reactivity difference between these two surface orientations. Table 2 shows that the rate constants for the two faces have comparable activation energies but that the pre-exponential factors for the prism plane reactions are larger than those on the basal plane.

The finding that H atom addition to CH_2 is the slow step in methane production may reflect rearrangement of the carbon bonding orbitals from the non-hybridized type in CH_2 to the fully hybridized type in the surface methyl radical. None of the free radicals CH, CH_2, or CH_3 were found to be emitted from the surface. Apparently carbon-hydrogen compounds are strongly bound to the graphite surface until a stable gas phase hydrocarbon is formed. These then leave the surface immediately.

Contrary to the graphite-oxygen reaction, the temperature dependence of the graphite-hydrogen product distribution shown in Fig. 5 appears to conform fairly well with Stickney's[14] quasi-equilibrium model of surface reactions.

-21-

B. Hydrogen Diffusion in Graphite

The fact that both the thick and thin basal plane targets are satisfactorily modeled as semi-infinite media in the molecular beam experiment permits an upper bound on the diffusivity of hydrogen in graphite at 2000°K to be computed. Eq. (8) represents a concentration wave decaying with depth of penetration into the solid oscillating about the steady value C_o. The characteristic decay constant is $(D/\omega)^{1/2}$. If the target thickness is more than about three decay constants, the wave is damped out before the concentration perturbation set up by the modulated beam on the front face reaches the rear face of the target. This criterion may be expressed quantitatively by:

$$h > 3(D/\omega)^{1/2} \tag{17}$$

where h is the target thickness. For $h = 25\mu m$ and a chopping frequency of 20 Hz ($\omega = 126$ rad/sec), Eq. (17) indicates that $D < 10^{-4} cm^2/sec$.

A similar test on the prism plane orientation was not possible because of the difficulty of fabricating very thin specimens of this orientation.

C. Extrapolation to High Hydrogen Pressures

Prior to the present study, all chemical kinetic investigations of the carbon-hydrogen system have utilized conventional techniques and high hydrogen pressures. We have attempted to ascertain whether the reaction model proposed here is consistent with these data. To do this, we use the model and its numerical rate constants to predict the carbon gasification rate in 1 atm of hydrogen. This pressure is in the middle of the range of pressures

tested in previous conventional kinetic studies. Because of the
high H_2 pressure, even a small H_2 sticking probability may
contribute significant amounts of atomic hydrogen to the
adsorbed layer on the surface. The conventional experiments are
conducted at steady state, so that bulk solution-diffusion is
absent (the solid is saturated with hydrogen during the
experiments). The steady state form of Eq. (5), with the supply
term supplemented with a contribution due to dissociative
adsorption of H_2 and the diffusion term omitted, is rewritten in
terms of the surface concentration of hydrogen:

$$\frac{n p_H}{(2\pi m_H kT)^{1/2}} + \frac{2\, \eta' p_{H_2}}{(2\pi m_{H_2} kT)^{1/2}} = 2k_2^e n^2 + 2K_1^2 k_2 n^2 + 4K_1 K_2 k_3 n^3 \qquad (18)$$

where η' is the sticking probability of molecular hydrogen and
m_H and m_{H_2} are the masses of the hydrogen atom and molecule,
respectively. Assuming that gas phase dissociation of hydrogen
is in equilibrium according to the reaction $1/2 H_2(g) = H(g)$, the
partial pressure of atomic hydrogen is given by:

$$p_H = K_p (p_{H_2})^{1/2} \qquad (19)$$

where K_p is the equilibrium constant for hydrogen dissociation.
Assuming the reaction surface to be equally divided between basal
and prism plane orientations, the rate constants on the right hand
side of Eq. (18) are taken to be the averages of those given in
Table 2 for the two surfaces. The atomic hydrogen sticking
probability is also taken to be the average of the values
determined for the basal and prism planes. Assuming a value of η'

and setting p_{H_2} = 1 atm, Eq. (18) is solved for n and the carbon removal rate is computed from:

$$\text{rate} = 2K_1^2 k_2 n^2 + K_1 K_2 k_3 n^3, \text{ carbon atoms/cm}^2\text{-sec} \qquad (20)$$

In order to compare the model predictions with past data, the apparent first order rate constant is calculated by equating the right hand sides of Eqs. (1) and (20). The model predictions are compared to the conventional kinetic data in Fig. 19. The relevant information for the data on this graph is summarized in Table 3 and additional details are available in ref. (5). Although it would not be difficult to find a curve which passed somewhere through the very scattered data on the graph, the theoretical curve for η' = 0 fits the best. The significance of the comparison shown in Fig. 19 is twofold. First, the model determined by the low pressure (5×10^{-4} torr) molecular beam experiment using atomic hydrogen as reactant can be extrapolated to predict gasification rates at H_2 pressures which are six orders of magnitude larger without any adjustments of the model. Second, the fact that η' = 0 is adequate to fit the older data substantiates the model proposed by Clarke and Fox[15], who attributed all reaction to the dissociated fraction of the reactant hydrogen gas.

In most reaction systems, extrapolation of a reaction model determined by low pressure molecular beam methods by six orders of magnitude in reactant gas pressure would be unsuccessful because the low pressure model would not be able to forsee coverage effects which become important at high pressures. However,

because of the very low sticking probability of molecular hydrogen, the H atom coverages of the surface calculated by Eqs. (18) and (19) for p_{H_2} = 1 atm are found to be of the same order of magnitude as those in the molecular beam experiment, namely <0.1% of a monolayer. This aspect of the theory, although it confirms the applicability of the model at high H_2 pressures, conflicts with other adsorption studies of hydrogen on graphite[16,17]. These studies found significant hydrogen adsorption on isotropic graphite at pressures less than 1 atm H_2 up to temperatures as high as 1500°C. However, it is difficult to distinguish adsorption from absorption in conventional experiments. In addition, the hydrogen adsorption experiments were performed on a porous graphite while the mechanism deduced in this study is based upon high density pyrolytic graphite. The internal porosity of ordinary graphite may contribute appreciable surface area not detectable by the BET method of determining specific surface areas of powdered specimens. In any case, the high temperature region of Fig. 19 is free from coverage complications and the agreement between the model proposed and the conventional kinetic data is adequate.

D.   Comparison with the Results of Wood and Wise

Wood and Wise[18] investigated the reaction of atomic hydrogen produced by a microwave discharge with isotropic graphite. The results agree with ours and with Rosner's[9] in showing a marked decrease in the methane production at temperatures above ∿800°K. Their explanation for this effect, that recombination

of surface hydrogen to form H_2 begins to dominate CH_4 formation

in this temperature region, is also similar to ours. However,

the reaction probabilities computed from their data are about

two orders of magnitude larger than those reported by Rosner[9] and

found in the present study. The mechanism Wood and Wise proposed

visualizes the prism plane surface to be fully saturated with hydrogen at

all times. The most exposed carbon atoms on the surface bind

two H atoms, the next layer binds one, and all subsequent layers

are not attached to hydrogen atoms. Their mechanism can be

written as:

sticking of H: $\quad -C-CH-CH_2 + H(g) \longrightarrow C-CH-CH_3 \qquad$ (A)

recombination: $\quad -C-CH-CH_3 + -C-CH-CH_3 \xrightarrow{\quad k_2 \quad} -C-CH-CH_2$

$$+ -C-CH-CH_2 + H_2(g) \qquad \text{(B)}$$

methane production: $\quad -C-CH-CH_3 + H_2(g) \longrightarrow -C-CH_2 + CH_4(g) \quad$ (C)

surface resaturation: $-C-CH_2 + H \xrightarrow{\quad fast \quad} -CH-CH_2 \qquad$ (D)
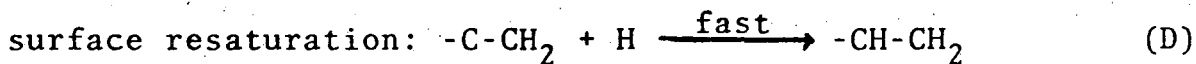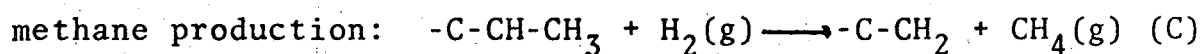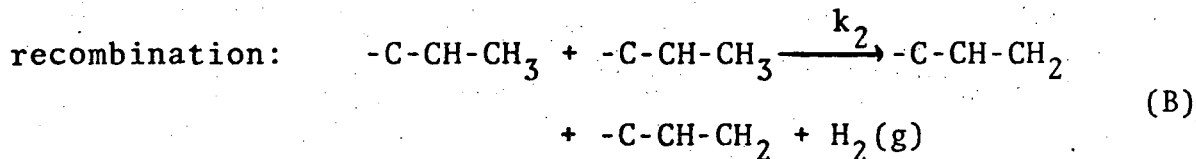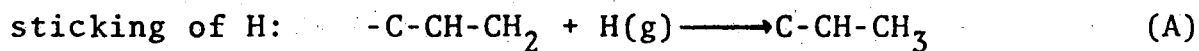
In reaction (A), an impinging H atom strikes the surface

and is adsorbed by a surface CH_2 group to form the CH_3 complex

shown on the right hand side. Recombination is effected by

removal of H_2 from adjacent CH_3 complexes, as shown in reaction

(B). Alternatively, Wood and Wise propose that an impinging H_2

molecule can strike the CH_3 complex and remove methane (reaction

(C)). The hydrogen-saturated surface is restored by rapid

hydrogen adsorption (reaction (D)). Assuming that the surface

CH_3 complex concentration is maintained by a balance of reactions

(A) and (B) (i.e., that reaction (C) is a negligible drain on the

CH$_3$ complex population) and using this concentration in the methane forming step (reaction (C)), the steady state rate of methane production is given by:

$$R_{CH_4} = kp_{H_2}p_H^{1/2} \qquad (21)$$

where the rate constant k is a composite of the elementary kinetic constants of reactions (A-C).

We have attempted to fit our data on methane formation to the model proposed by Wood and Wise. Since the surface is always saturated with hydrogen in this mechanism, there is a fixed density N$_s$ of CH$_2$ groups capable of accepting an H atom to form the CH$_3$ complex. Following the Wood-Wise analysis, the fraction θ of the available CH$_2$ sites which contain an extra H atom (i.e., which are CH$_3$ complexes) is assumed to be very much less than unity. The sticking probability η now refers to the probability that an impinging H atom strikes a CH$_2$ group and converts it to a CH$_3$ complex. Similarly, and H$_2$ molecule impinging upon a CH$_3$ complex has a probability η' of converting it to methane. The time dependent surface mass balance on the CH$_3$ complex is:

$$N_s \frac{d\theta}{dt} = \eta I_o g(t) - 2k_2\theta^2 - \eta' I_o' \theta g(t) \qquad (22)$$

where k$_2$ is the rate constant for reconstitution of H$_2$ from adjacent CH$_3$ complexes and I$_o'$ is the flux of molecular hydrogen in the primary beam. Following Wood and Wise, the last term on the right hand side of Eq. (22) is assumed to be negligible compared to the recombination terms (although with a measured reaction probability of $\sim$0.1, this does not appear to be a very

sound simplification). The resulting equation can be solved by substitution of Eq. (6) for the gating function and:

$$\theta(t) = \theta_0 + \bar{\theta}_1 e^{i\omega t} \tag{23}$$

for the CH_3 complex coverage. Following the method outlined earlier in this paper, we solve for θ_0 and $\bar{\theta}_1$. The fundamental mode of the rate of methane formation per unit area is given by the last term on the right hand side of Eq. (22) with $g(t)$ and $\theta(t)$ replaced by Eqs. (6) and (23), respectively. This rate is referred to the fundamental mode of the rate of H atom impingement, $\frac{1}{2} I_0 g_1$, in order to produce the reaction product vector. Upon converting to polar form, the methane phase lag and apparent reaction probability predicted by the model of Wood and Wise are given by:

$$\tan\phi_{CH_4} = \frac{S}{3 + 2S^2} \tag{24}$$

$$\epsilon_{CH_4} = \left(\frac{3}{2\sqrt{2}}\right) \eta \left(\frac{\eta' I'_o}{\eta I_o}\right) \left(\frac{\eta I_o}{2k_2}\right)^{1/2} F(S) \tag{25}$$

where:

$$F(S) = \frac{(1 + \frac{13}{9} S^2 + \frac{4}{9} S^4)^{1/2}}{1 + S^2} \tag{26}$$

and

$$S = \frac{\omega N_s}{2(\eta I_o k_2)^{1/2}} \tag{27}$$

In the dc limits (S = 0, F(0) =1), Eq.(25) reduces to Eq.(21) (except for the numerical factor $3/2\sqrt{2}$ = 1.06 which is the error introduced into the analysis by using the approximate method of solving Eq.(22)).

Eqs.(24) and (25) are the analogs of Eqs.(13) and (14) for the model of Wood and Wise. That this model does not fit our experiments can be seen most easily from the methane phase data. Eq.(24) predicts that the largest phase lag should be 11.5°, whereas the phase lags in Figs. 6, 7, and 11 are all larger than this value.

In requiring the methane formation step to be accomplished by molecular hydrogen (reaction (C)), the model of Wood and Wise implies that methane formation would not occur in a gas containing only atomic hydrogen. This intuitively unacceptable aspect of the model may be remedied by allowing atomic hydrogen to perform the same function as does H_2 in reaction (C). The only change in the theoretical results is replacement of I_0' by I_0 in Eq.(25). No better agreement between the present data and the model of Wood and Wise is obtained by this alteration.

ACKNOWLEDGEMENT

Table 1   H atom-Graphite Reaction Model

$H\ (g) \xrightarrow{\quad \eta \quad} H\ (ads)$ Sticking

$H\ (ads) \rightleftharpoons H\ (Sol'n)$ Bulk solution-diffusion

$H\ (ads) + H\ (ads) \xrightarrow{\quad k_2^e \quad} H_2\ (g)$ Recombination

$H\ (ads) + C \underset{\quad}{\overset{K_1}{\rightleftharpoons}} CH\ (ads)$ Surface equilibrium

(a)   (b)

$CH\ (ads) + H\ (ads) \underset{\quad}{\overset{K_2}{\rightleftharpoons}} CH_2\ (ads)$ $CH\ (ads) + CH\ (ads) \xrightarrow{\quad k_2 \quad} C_2H_2\ (g)$

$CH_2\ (ads) + H\ (ads) \xrightarrow{\quad k_3 \quad} CH_3\ (ads)$

$CH_3\ (ads) + H\ (ads) \xrightarrow{\quad Fast \quad} CH_4\ (g)$

Methane Branch   Acetylene Branch

(Low temperature)   (High temperature)
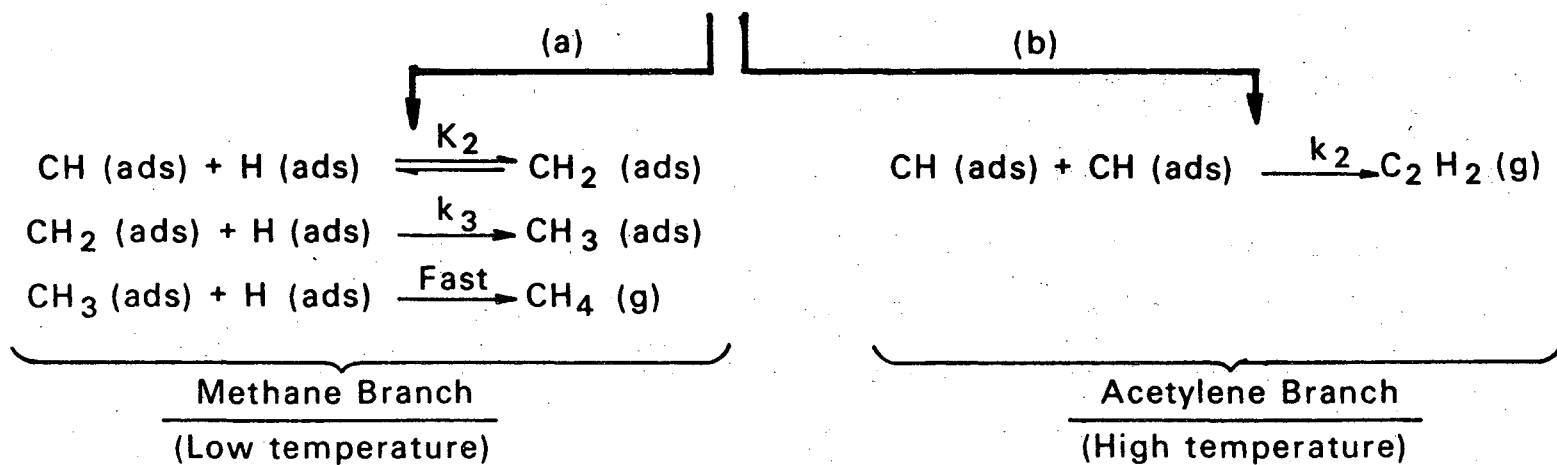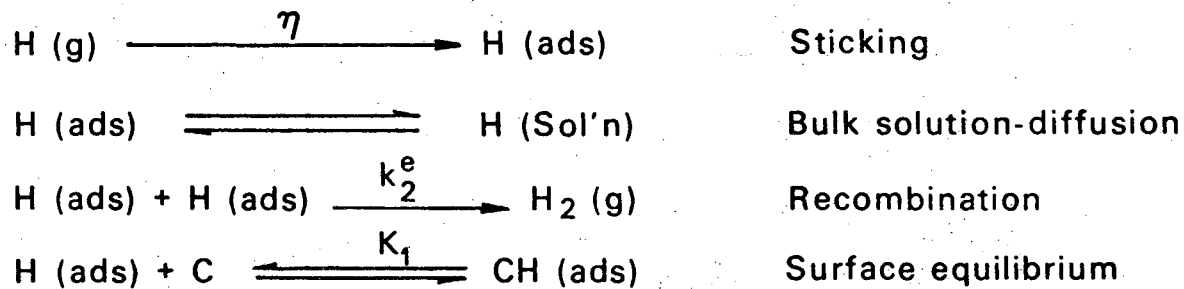
XBL755-4918

Table 3

SUMMARY OF KINETIC STUDIES ON THE HYDROGEN-CARBON SYSTEM

	Temperature range (°C)	Hydrogen pressure Range	Form of Carbon	Specimen Geometry	Order of Reaction	Activation energy (kcal/mole)	Mode of Analysis
(a) C. W. Zielke, E. Gorin, Ind. and Eng. Chem. 47, 820 (1955)	820-930	10-30 atm	"disco" char	packed bed; 2cm high, 3cm diam.	1-1.5	23 at 30 atm and 0% gasification; 10-15 after 0-60% gasification	Weight loss
(b) J. D. Blackwood, Aust. J. Chem. 15, 397 (1962)	650-870	1-40 atm	coconut-shell char	packed bed; 10cm high	≈1.0	41 at 30 atm	Analysis for CH_4
(c) P. G. Salgado, Ph.D. Dissertation, West Virginia Univ. (1958)	1000-1400	1 atm	nuclear grade graphite	Rectangular block	≈1.0	30	Weight loss
(d) N. S. Corney, R. B. Thomas, AERE-C/R-2502, (1958)	560-800	400-800 torr	nuclear grade graphite	Tube: 20cm long, 1cm id, 0.5cm thick	≈1.0	65 at 600-800°C; 10 at lower temp. (<600° C)	Analysis for CH_4, gas chromatography
(e) R. G. Breckenridge, J. C. Bowman, in R. Lowrie, USAEC Rept.NP-10401, Semi-Annual Progress Report, Union Carbide, Tarrytown, N.Y., (1961)	1895-2370	5 torr	nuclear grade graphite	Filament		210 at 2136-3270°C; 74 at 1895-2000°C for C_2H_2	Analysis for C_2H_6 and C_2H_2
(f) R. Lowrie, USAEC Rept. NP-11311, Semi-Annual Progress Report, Union Carbide, Tarrytown, N.Y., Parma, Ohio, July 1-Dec. 31, 1961	2300-2370	4-12 torr for pressure-dependence expt., ≈1 atm for corrosion rate expt.	Various grades of graphite	Cylinder	≈1.0 for carbon loss ≈1.0 for C_2H_8		Weight loss; Analysis for propane.
(g) D. P. Macmillan, Nucleonics, 19, 85 (1961)	Up to 2600		Commercial graphite			31, T>2200°C 10, T<2200°C	
(h) E. A. Gulbransen, K. F. Andrews, F. A. Brassart, J. Electrochem. Soc. 112, 49, (1965)	1200-1650	10-38 torr	Spectro-scopic graphite	Cylinder; 0.5cm high, 0.3cm diam.		72	Weight loss and mass spectrometric analysis of gases.
(i) K. Hedden, in Proc. Conf. on Carbon, The Macmillan Co., pp.125-131, NY (1962)	1000-1250	10-100 atm	Spectro-scopic carbon.	Packed bed; 5cm high, 2cm diam.	1.0	85	Gas analysis
(j) J. T. Clarke, B. R. Fox, J. Chem. Phys. 46, 827 (1969)	1700-3100	0.01-1.0 atm	graphite	Filaments, 0.2 and 0.5mm diam.	1.0	51	
(k) J. W. H. Chi, C. E. Landahl, Nucl. Appl., 4, 159 (1968)	1500-2500	11-56 atm	Pyrographite	Flat-plate coupons	1.0	47 (CH_4) 86 (C_2H_2)	Weight loss

-31-

TABLE 2

KINETIC CONSTANTS FOR THE HYDROGEN-GRAPHITE REACTION

Process	Rate Constant (units)	Prism Plane*	Basal Plane*
Sticking of H	η	0.02	0.006
Recombination (H_2)	k_2^e (cm^2/atoms-sec)	$1.06 \times 10^{-2} \exp[- \frac{15.9}{RT_S}]$	$1.30 \times 10^{-4} [- \frac{18.5}{RT_S}]$
CH_4 Production	$K_1 K_2 k_3$ (cm^4/atoms^2-sec)	$1.27 \times 10^{-18} \exp[- \frac{3.3}{RT_S}]$	$2.17 \times 10^{-21} \exp[\frac{0.9}{RT_S}]$
Bulk Solution-Diffusion	$H\sqrt{D}$ (sec$^{-1/2}$)	$2.70 \times 10^6 \exp[- \frac{9.6}{RT_S}]$	$3.85 \times 10^4 \exp[- \frac{5.4}{RT_S}]$
C_2H_2 Production	$K_1^2 k_2$ (cm^2/atoms-sec)	$1.59 \exp[- \frac{32.5}{RT_S}]$	$1.82 \times 10^{-3} \exp[- \frac{26.8}{RT_S}]$

*Activation energies in kcal/mole, surface temperature in °K x 10^{-3}.

REFERENCES

1. M. Bertholet, Ann. Chim, Phys. 67, No. 3, 52 (1863)

2. R. M. Barrer and E. K. Rideal, Proc. Roy. Soc., 149A, 231 (1935)

3. R. M. Barrer, Trans. Farad. Soc. 32, 481 (1936)

4. R. M. Barrer, J. Chem. Soc. (London), Part II, 2, 1256 (1936)

5. R. A. Krakowski and D. R. Olander, ERDA Report UCRL-19149 (1970)

6. D. R. Olander, W. Siekhaus, R. Jones and J. A. Schwarz, J. Chem. Phys. 57, 408 (1972)

7. R. H. Jones, D. R. Olander, W. J. Siekhaus and J. A. Schwarz, J. Chem. Phys., 57 421 (1972)

8. R. H. Jones, D. R. Olander, W. J. Siekhaus and J. A. Schwarz, J. Vac. Sci. Technology, 9, 1429 (1972)

9. D. E. Rosner and H. D. Allendorf, Heterogeneous Kinetics at Elevated Temperatures, p 231, Plenum Press (1975)

10. D. R. Olander, in "The Structure and Chemistry of Solid Surfaces", G. A. Somorjai, Ed., p 45-1, Wiley, New York (1969)

11. J. A. Schwarz and R. J. Madix, Surf. Sci., 46 317 (1974)

12. D. R. Olander and A. Ullman, submitted to Inter. J. of Chem. Kinetics.

13. G. A. Beitel, J. Vac. Sci. and Tech., 6, 224 (1968)

14. R. E. Stickney and J. C. Batty, J. Chem. Phys. 51, 4475 (1969)

15. J. T. Clarke and B. R. Fox, J. Chem. Phys. 46, 827 (1967)

16. W. J. Thomas, J. Chem. Phys. 58, 61 (1961)

17. J. P. Redmond and P. L. Walker, Jr., J. Phys. Chem. 54, 1093 (1960)

18. B. J. Wood and H. Wise, J. Phys. Chem., 73, 1348 (1969)

1.   Schematic of the modulated molecular beam-mass spectrometer method for investigating the graphite-hydrogen reaction.

2.   Detail of the atomic hydrogen source.

3.   Comparison of the performance of the hydrogen source with equilibrium theory. p_H is the partial pressure of atomic hydrogen in the oven and p_T is the total hydrogen pressure in the oven. K_p is the equilibrium constant for the reaction: $1/2 H_2(g) = H(g)$.

4.   Scanning electron micrographs of graphite sample. (a) basal plane after polishing, x10,000; (b) prism plane after polishing, x3000; (c) basal plane after reaction, x10,000; (d) prism plane after heating/reaction, x3000.

5.   Temperature dependence of the apparent reaction probabilities for methane and acetylene. Triangles and circles represent duplicate runs.

6.   Temperature dependence of the reaction phase lag for methane and acetylene. Triangles and circles represent duplicate runs.

7.   Phase-frequency scan at low temperature for methane. Triangles and circles represent duplicate runs.

8.   Variation of methane reaction probability with frequency. Triangles and circles represent duplicate runs.

9.   Phase-frequency scan for acetylene at high temperature.

10.   Variation of acetylene reaction probability with frequency.

11.   Variation of methane phase lag with beam intensity. The different symbols for the prism plane represent replicating runs.

12.   Variation of methane reaction proability with beam intensity. The different symbols for the prism plane represent replicating runs.

13.   Variation of acetylene phase lag with beam intensity.

14.   Variation of acetylene reaction probability with beam intensity.

15.   Effect of target thickness on the acetylene phase lag.

16.   Effect of target thickness on the acetylene reaction probability.

17. Hysteresis in the methane reaction probability.

18. Kinetic constants for the hydrogen-graphite reaction.

19. High pressure kinetics of the carbon-hydrogen reaction.
Dashed lines: extrapolation of molecular beam data to
P_{H_2} = 1 atm for various H_2 sticking probabilities;
solid lines and points: data from investigations described
in Table 3.

Fig. 1

Fig. 2

XBL755-4926

Hydrogen Dissociation

● Experiment
—— Theory

P_H/K_p^2
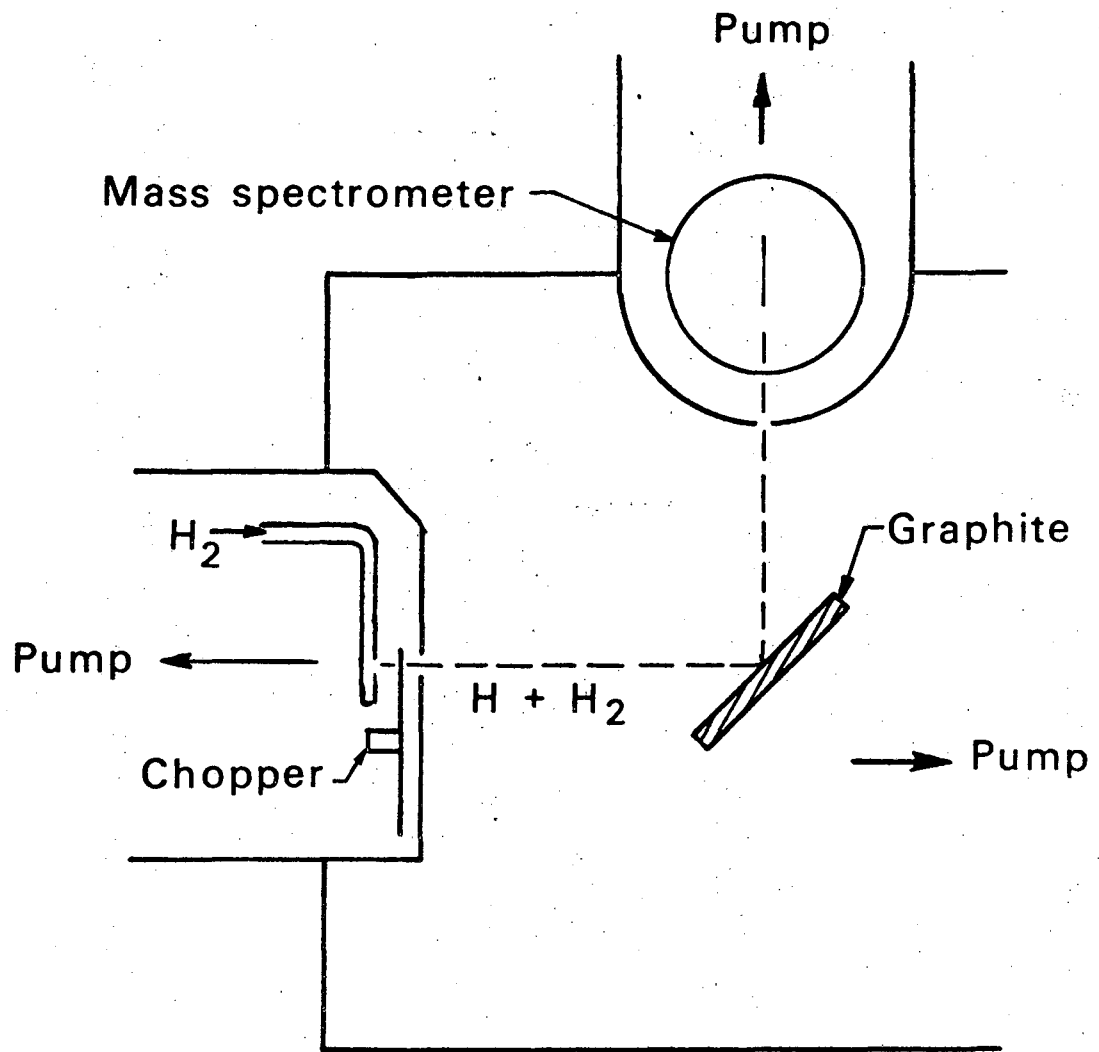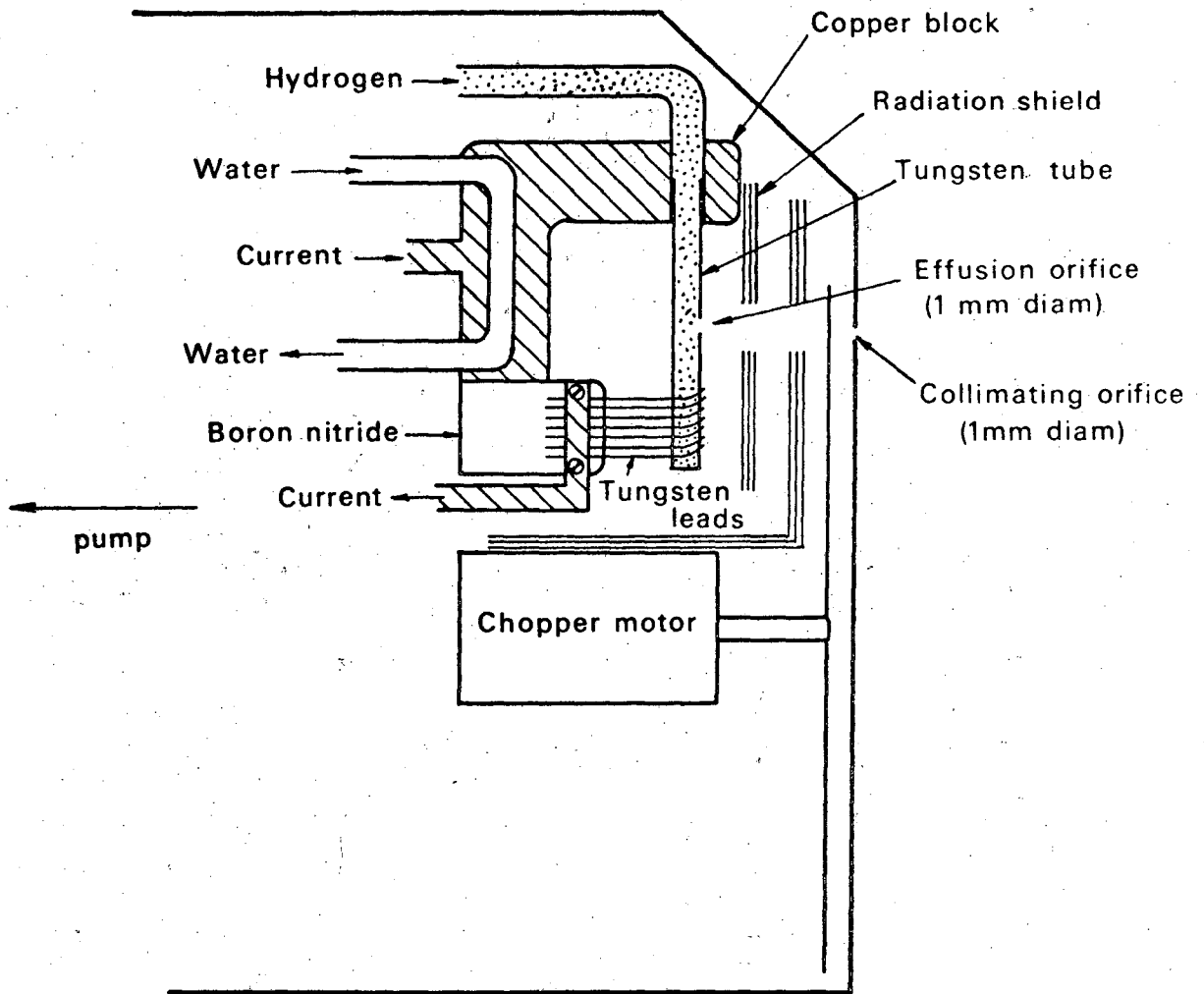
P_T/K_p^2
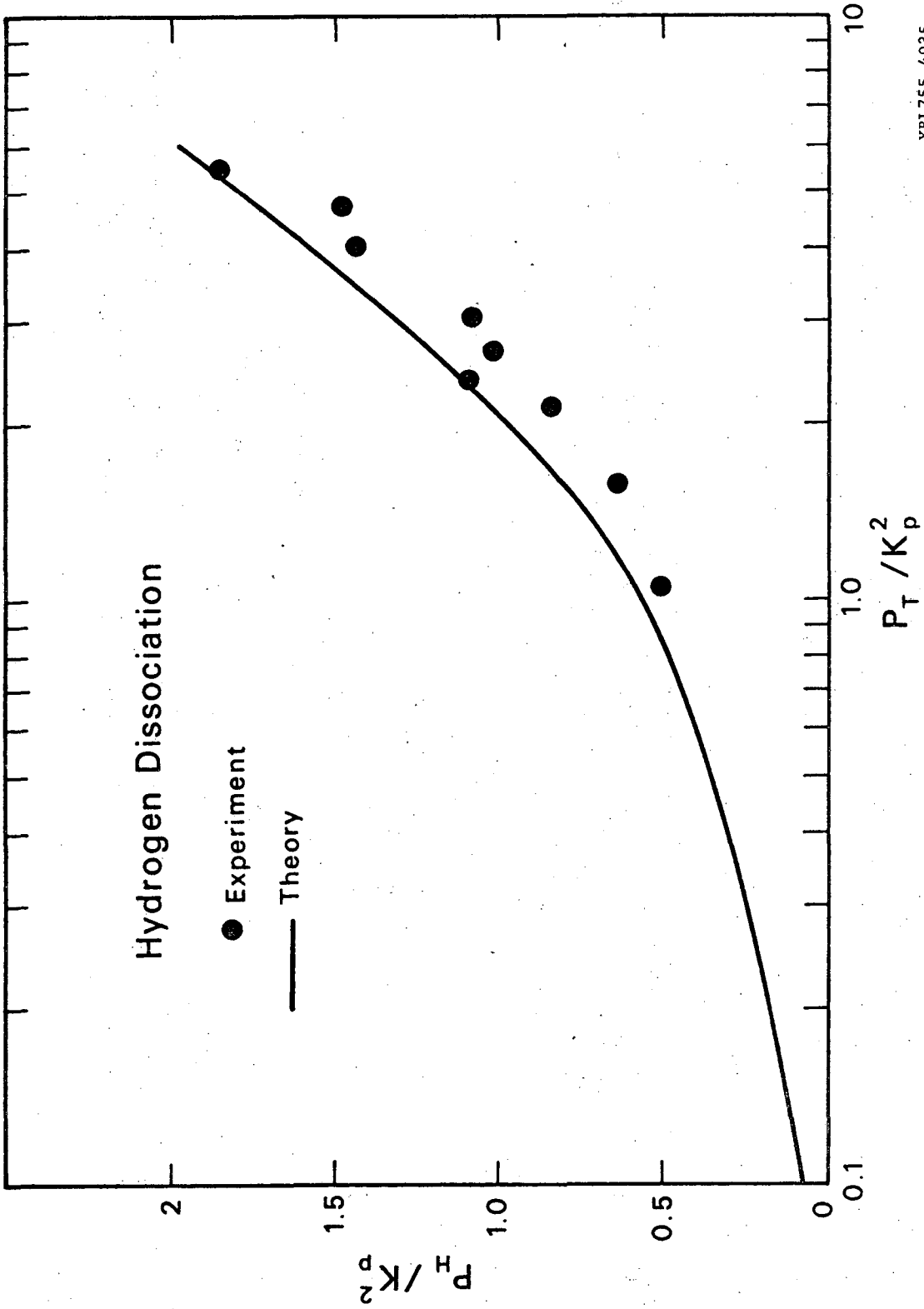
XBL755-4935

Fig. 3
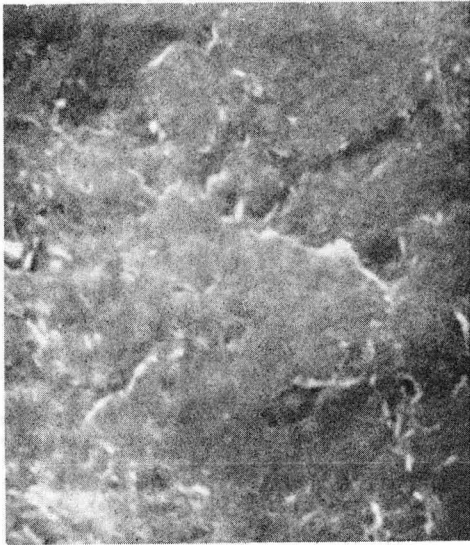
(a)
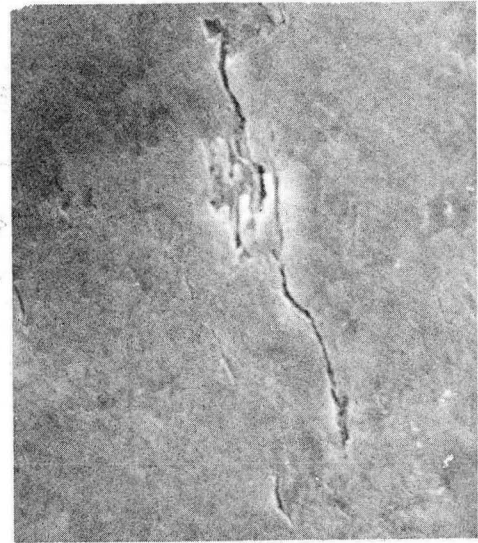
(b)
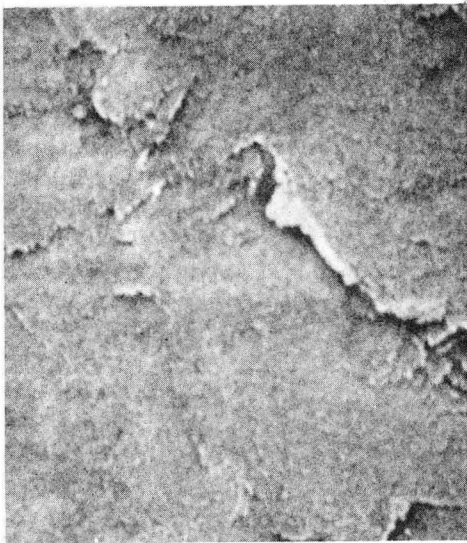
(c)

(d)
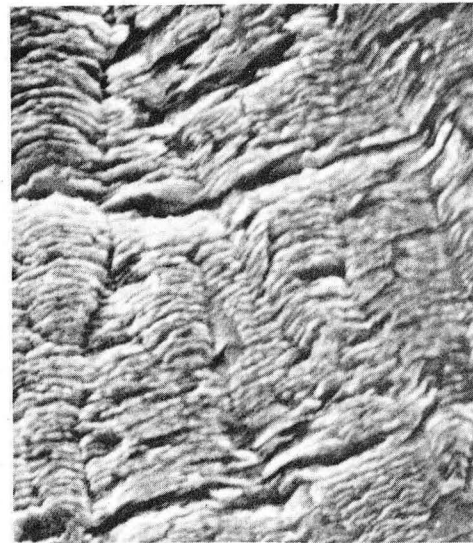
XBB757-5137
Fig. 4
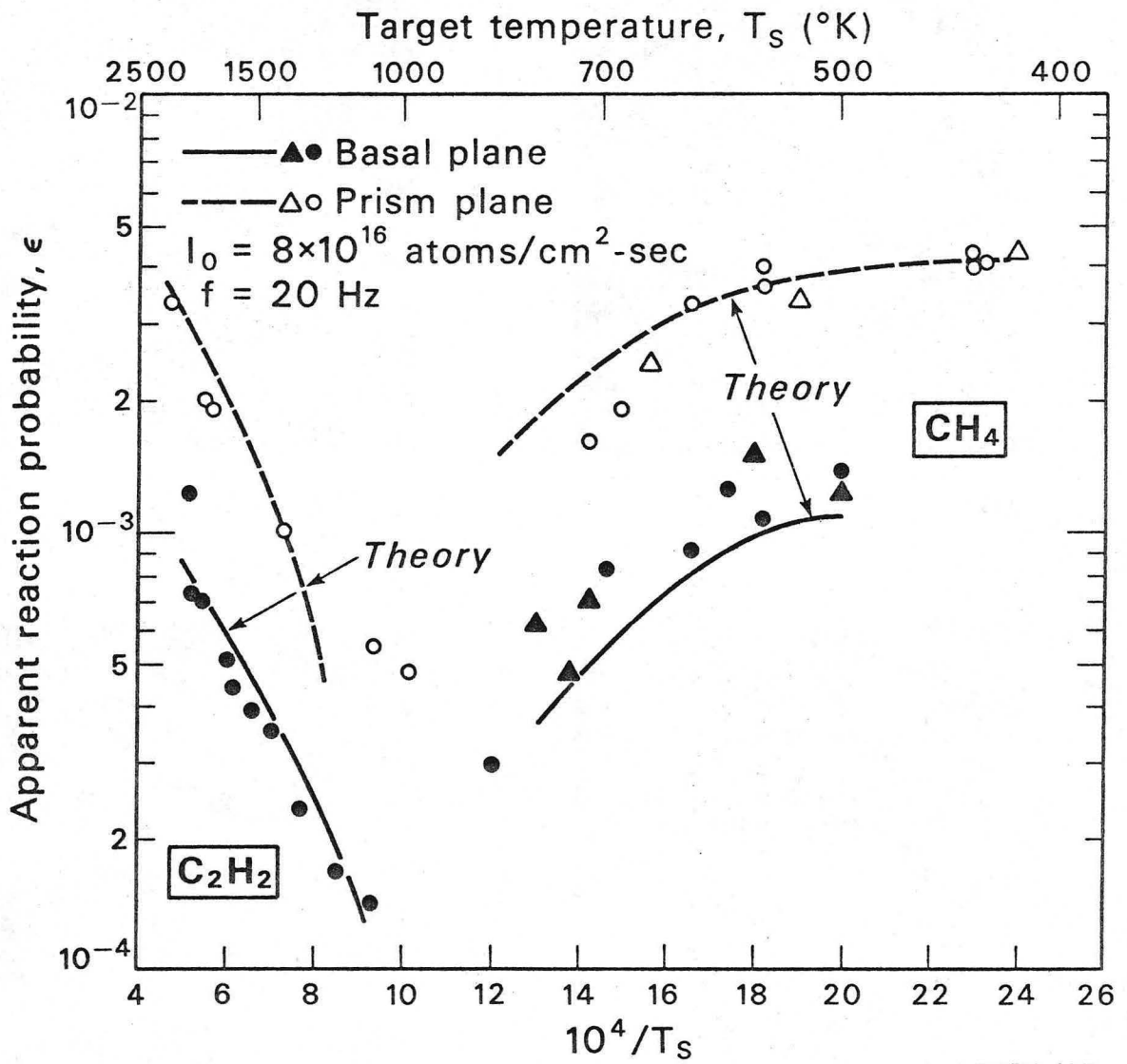
Fig. 5
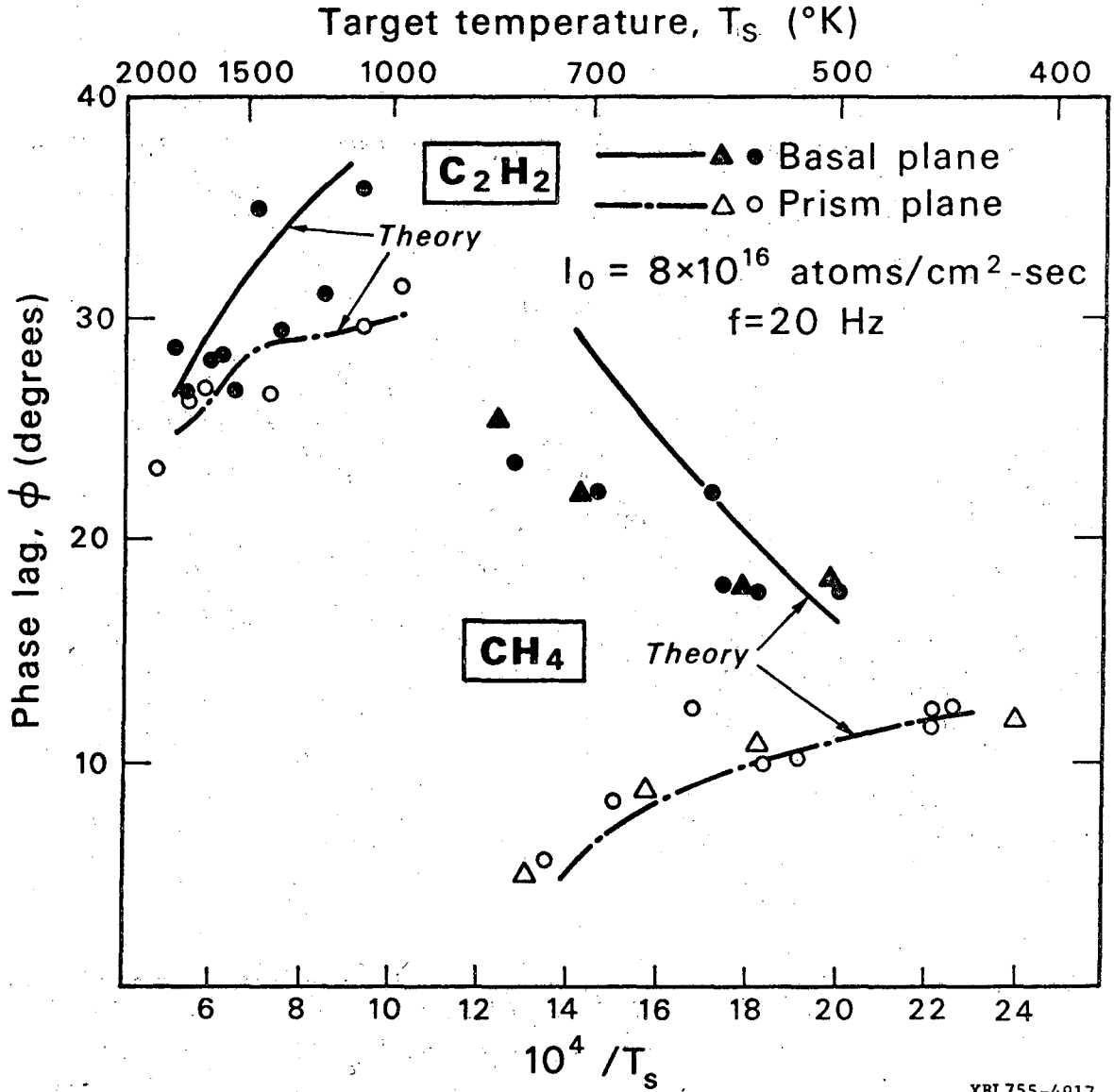
XBL755-4920

Fig. 6

XBL755-4922

Fig. 7

-42-
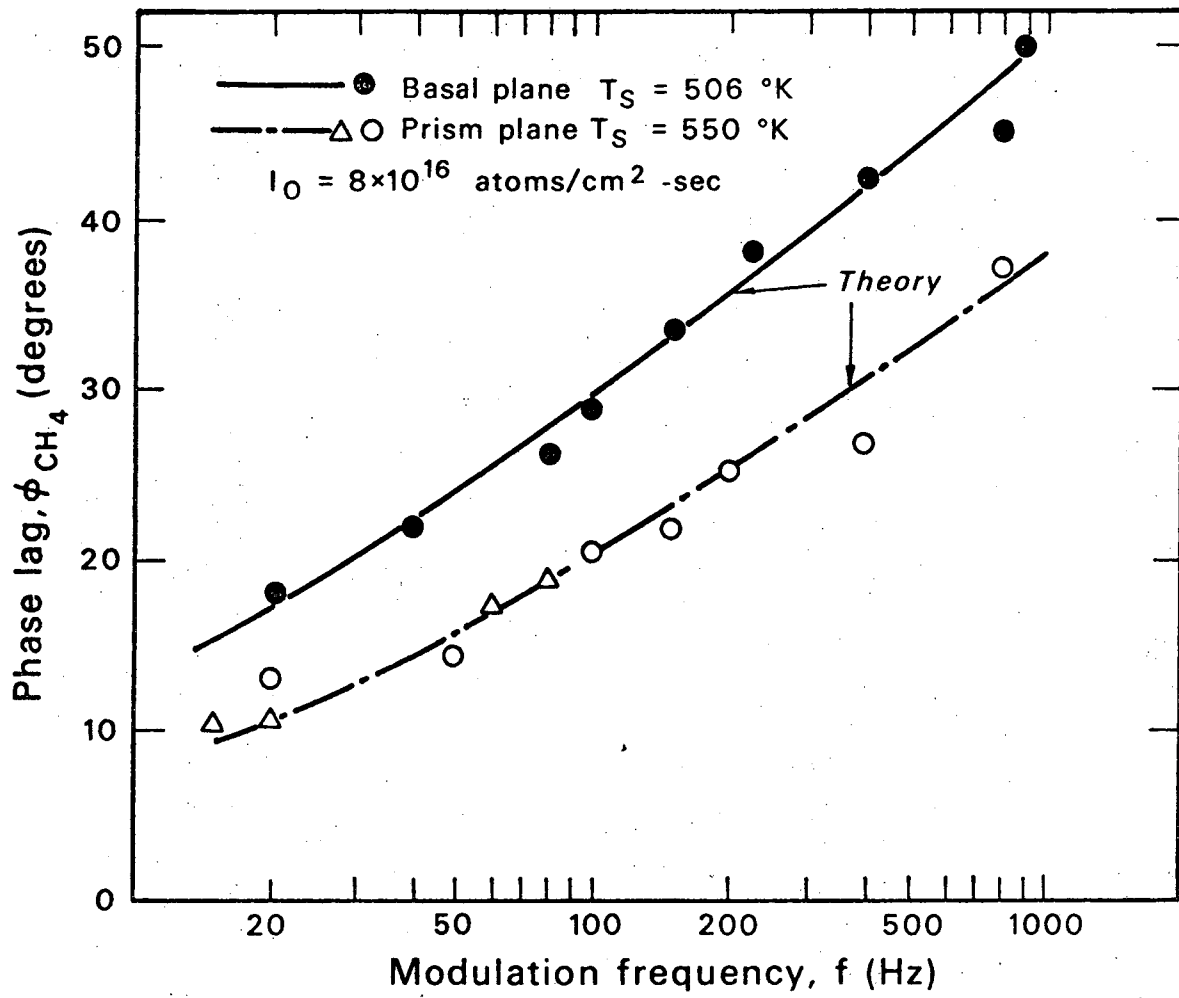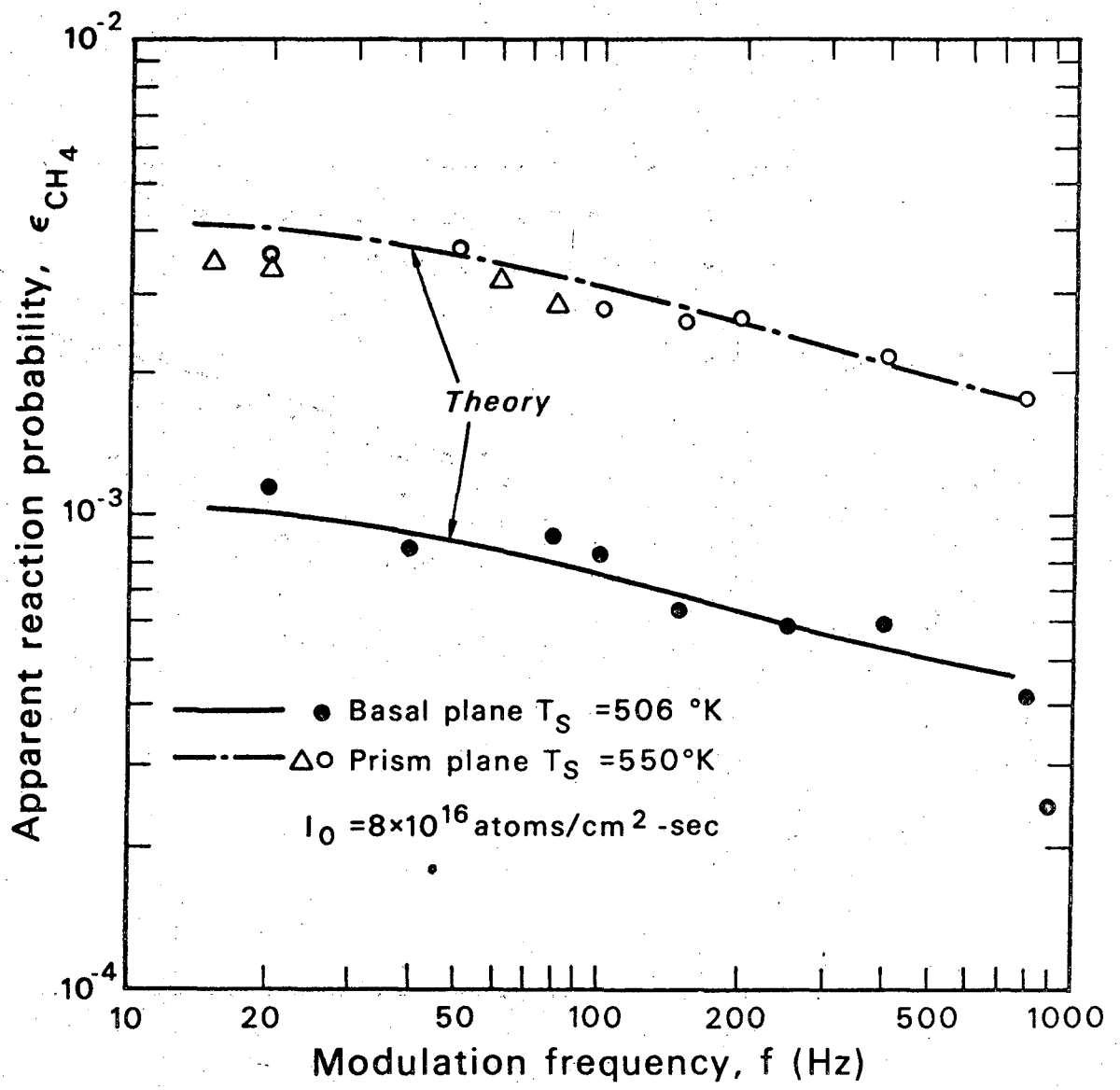
XBL755-4925

Fig. 8

XBL755-4923

Fig. 9

-44-
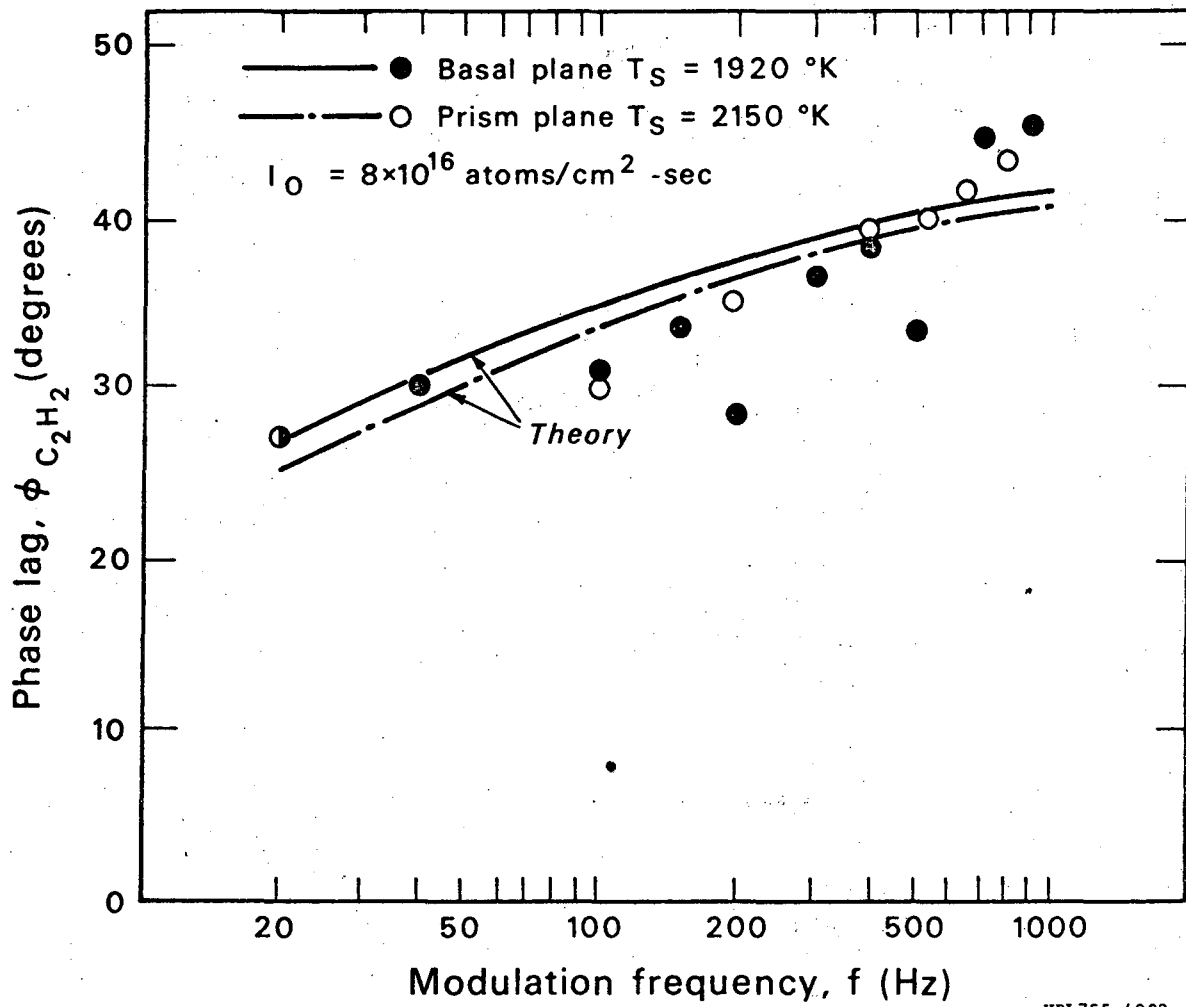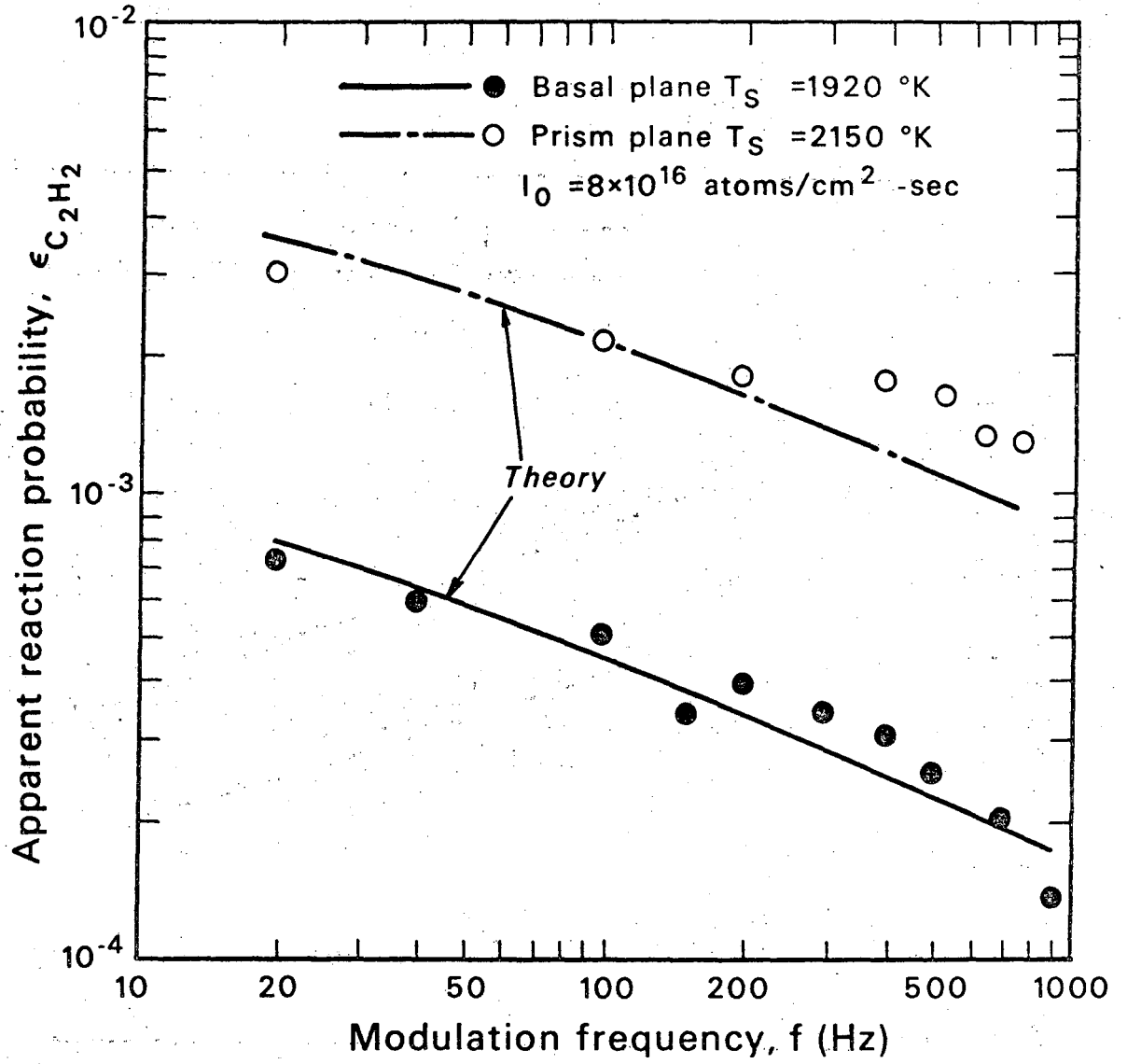
XBL755-4928

Fig. 10

XBL755-4921

Fig. 11

Fig. 12

XBL755-4924

Fig. 13

XBL755-4930

-87-

Fig. 14

Fig. 15

XBL755-4929

Target temperature, T_S (°K)

C$_2$H$_2$ Basal plane
$I_0 = 8 \times 10^{16}$ atoms/cm^2 -sec
f=20 Hz

● 1 mm thick
△ 2.5×10^{-2} mm thick

Apparent reaction probability, $\epsilon_{C_2H_2}$

$10^4/T_S$
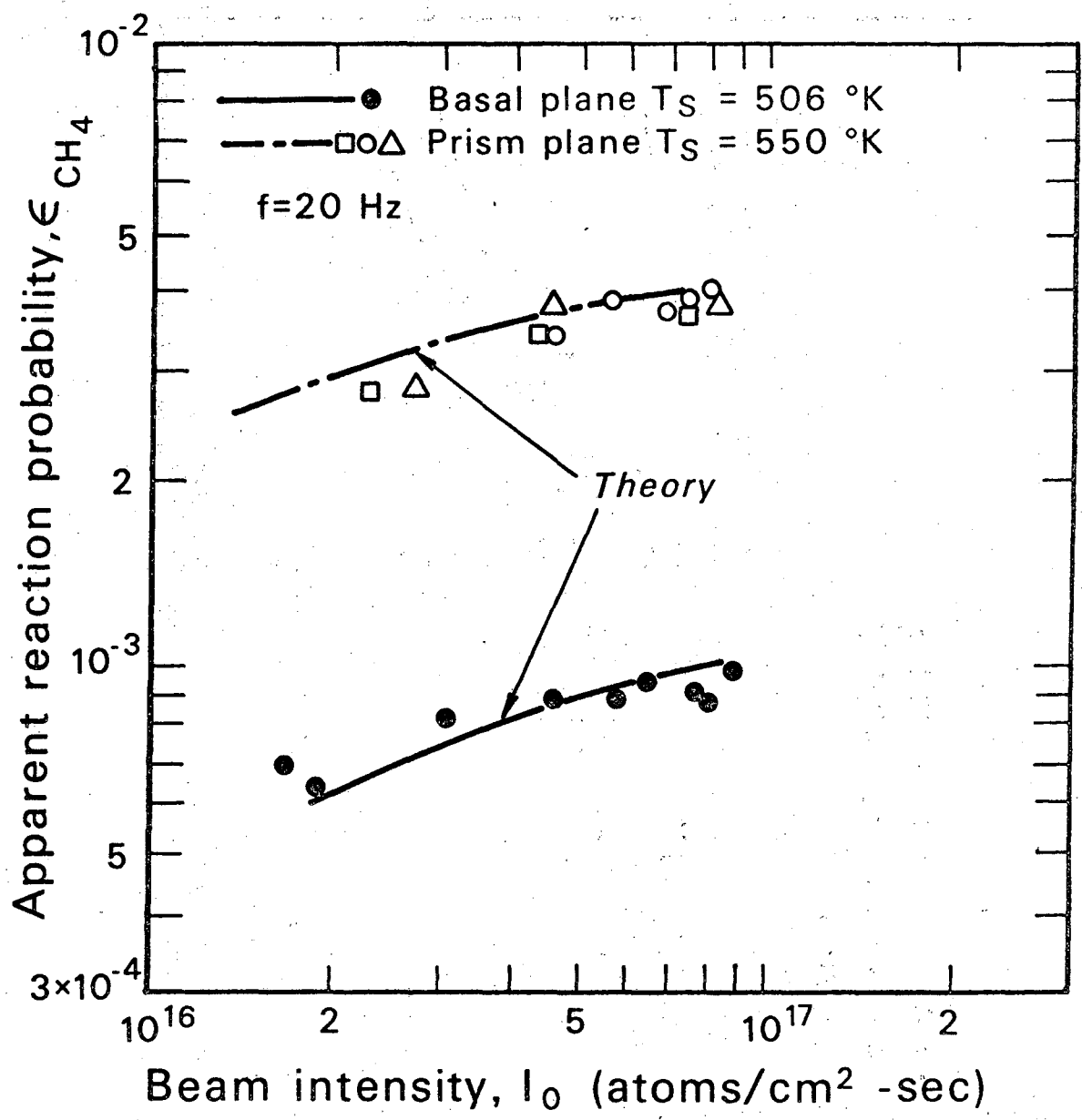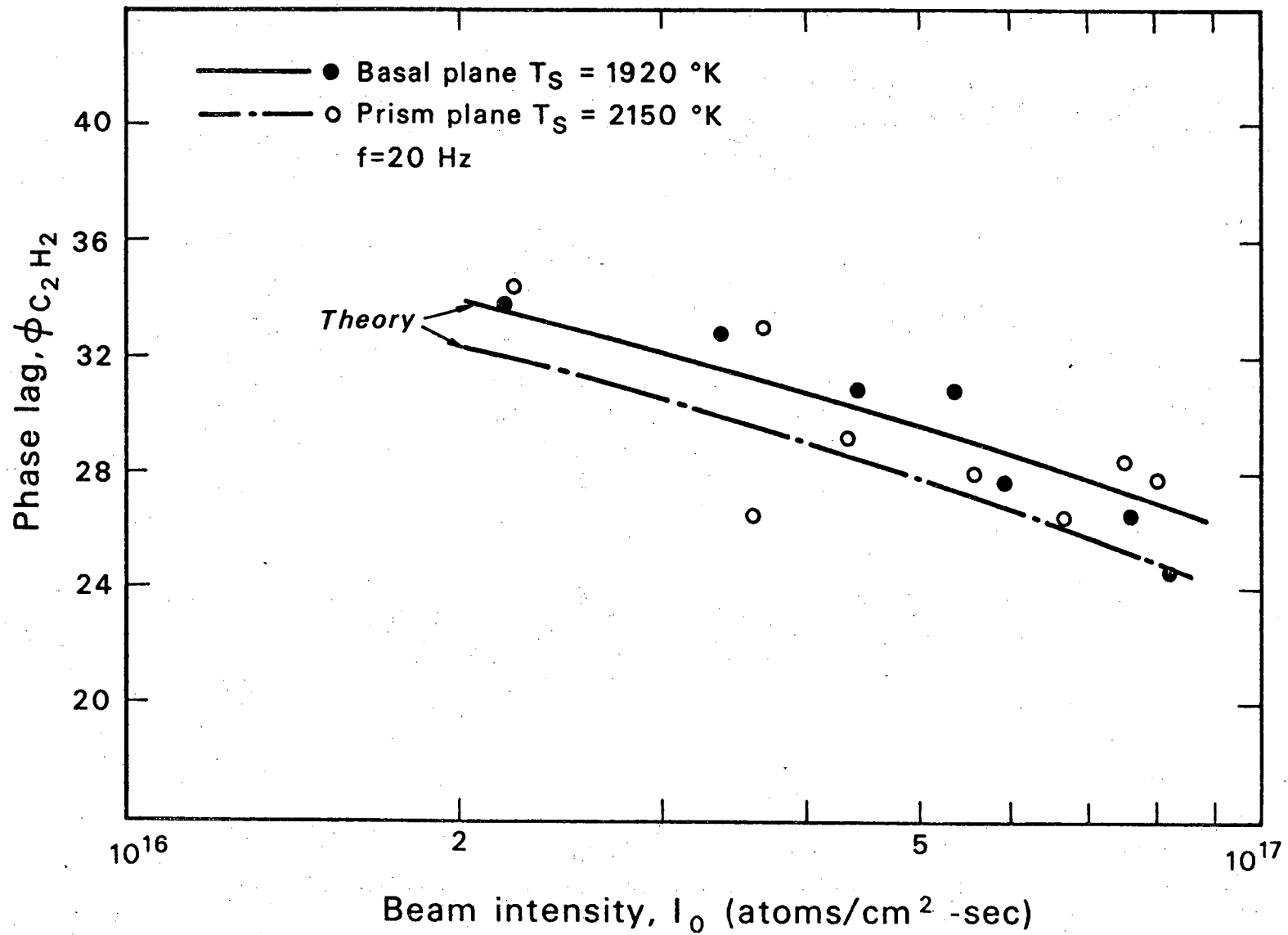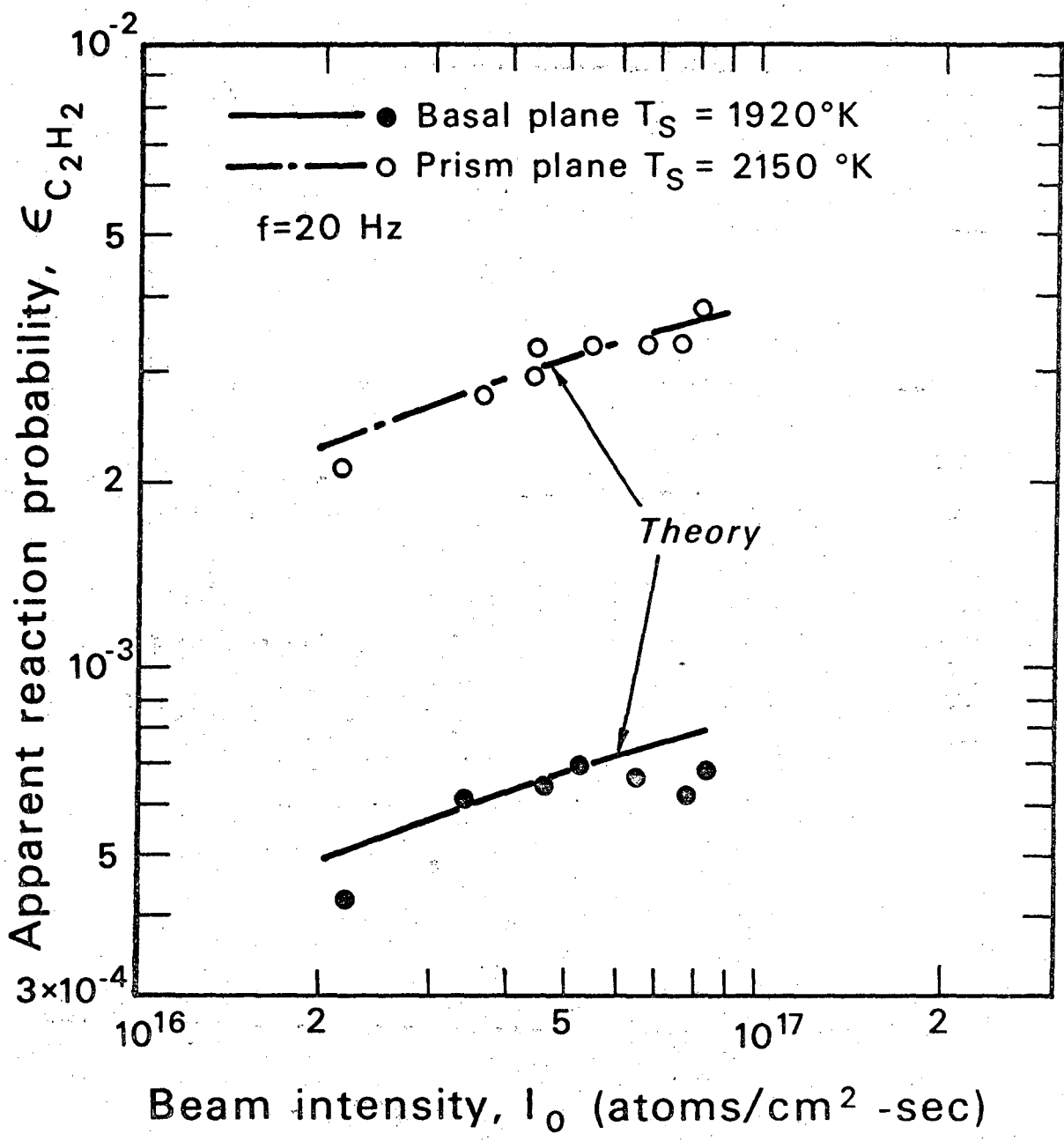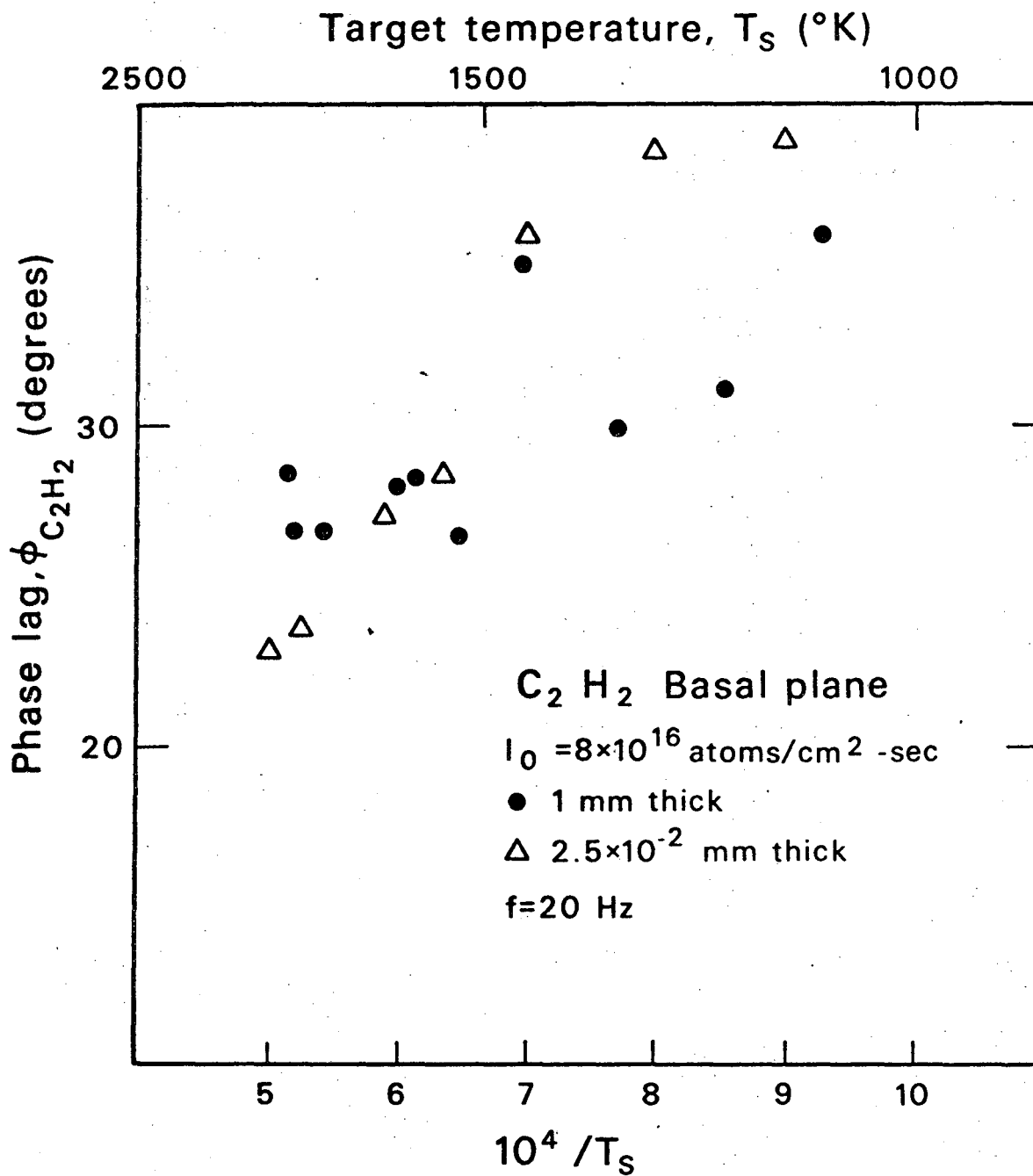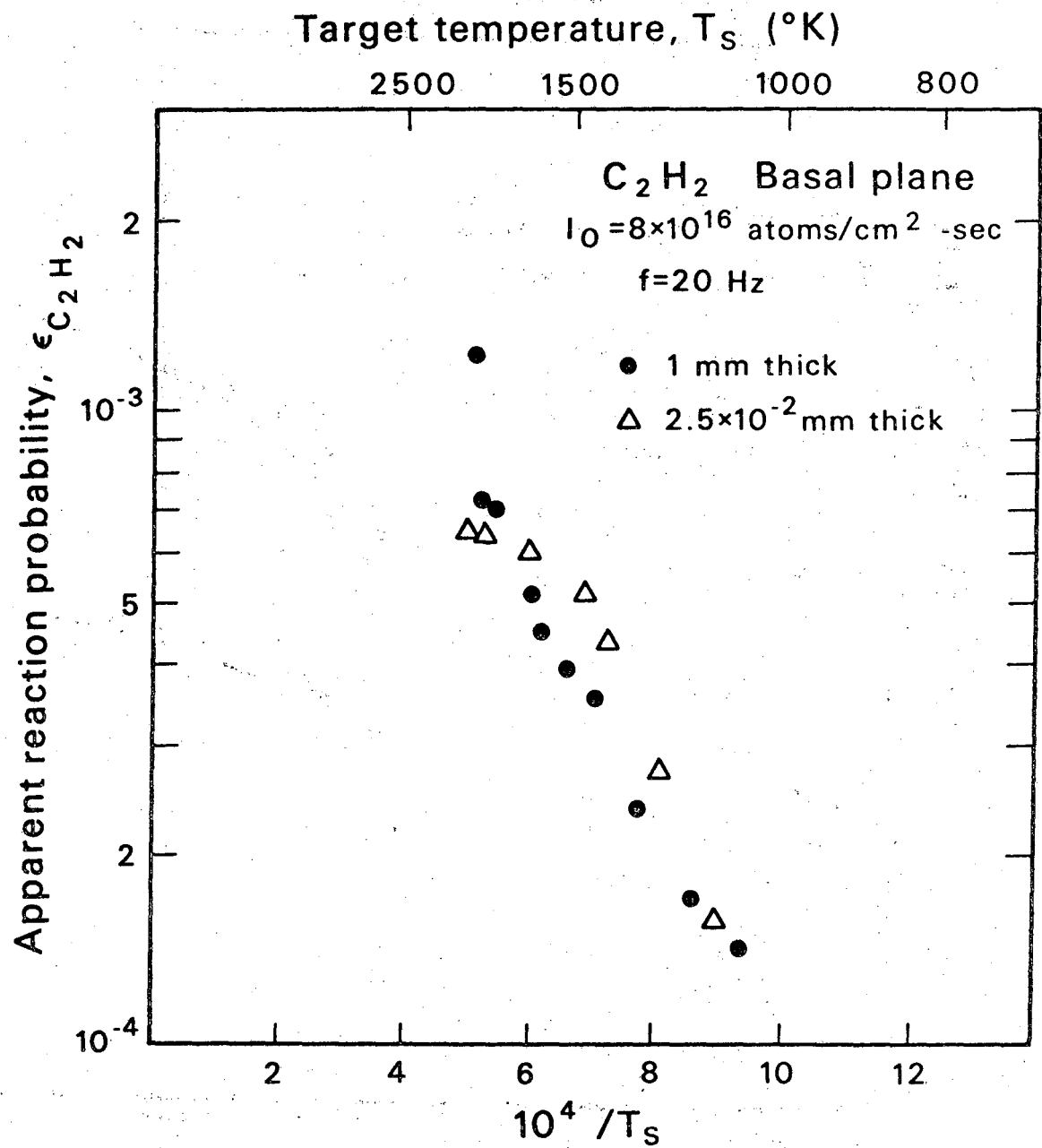
XBL755-4927

Fig. 16

XBL755-4932

Fig. 17

-52-

Fig. 18

XBL755-4919

XBL757-4404

Fig. 19

-54-